Experimental Characterization of the Compressive Behaviour of Gas Diffusion Layers in PEM Fuel Cells

by

Sogol Roohparvarzadeh

A thesis
presented to the University of Waterloo
in fulfillment of the
thesis requirement for the degree of
Master of Applied Science
in
Mechanical Engineering

Waterloo, Ontario, Canada, 2014

I hereby declare that I am the sole author of this thesis. This is a true copy of the thesis, including any required final revisions, as accepted by my examiners.

I understand that my thesis may be made electronically available to the public.

Abstract

Successful commercialization of polymer electrolyte membrane (PEM) fuel cells is highly dependant on performance of the membrane electrode assembly (MEA). The performance of the gas diffusion layer (GDL) of the MEA is highly influenced by applied compressive load. Compression of the GDL changes its porosity and microstructure, which will consequently change the physical properties of the GDL. Hence to improve the properties of the GDL, understanding its compressive behaviour is crucial.

In the present study, the compressive behaviour of the GDL is characterized by performing a series of compression tests using a compression apparatus. The compressive test is first performed on an untreated carbon paper by measuring its thickness as a function of compressive load at room temperature. The obtained results are analyzed and presented in a compressive stress-strain curve. The compressive stress-strain curve of the GDL is divided into 3 distinct regions. The first region represents the stress-strain behaviour at very low stress values. In this region, the compressive strain of the GDL increases rapidly and linearly with the applied stress. In the second region, the compressive strain increases less rapidly and non-linearly with applied stress. In the last region, the compressive stress-strain behaviour becomes linear again, but the strain increases at a lower rate. Analysis of the SEM images for both compressed and uncompressed GDL samples suggest that the stress-strain behaviour of the GDL in the first two regions is induced by the surface roughness and local thickness variations.

The compressive behaviour of the GDL is further analyzed by investigating the effect of temperature, relative humidity, and hydrophobic treatment. The compressive stress-strain curves obtained at temperatures of 25°C, 45°C, 65°C, and 85°C are almost identical within the experimental margin of error, which suggests that fuel cell's operating temperature has no appreciable effect on the compressibility of the GDL. The compressive stress-strain curve obtained from compressive test at humidified environment shows a higher change in strain in the second region of the curve. The study on the effect of Polytetrafluoroethylene (PTFE) coating on compressibility and pore distribution shows that increase in PTFE content decreases the overall pore volume of the GDL and hence decreases the compressibility.

At last, the effect of cyclic loading is studied by measuring the thickness of GDL samples during 2500 loading/unloading cycles. The strain of the GDL samples increases by 50% after the samples undergo 2500 cycles of compression. The effect of unloading was further investigated by measuring the thickness of the sample as a function of applied compressive load while loading the sample by compression pressures of up to 3.5MPa and

then unloading the sample to zero MPa for seven cycles. It is found that the structure of the GDL degrades significantly under compression cycles. This study concludes that the compressive behaviour of the GDL under cyclic compression is a major drawback and without further improvements, the required durability will not be achieved.

Acknowledgements

I would like to first express my deepest gratitude to Professor Xianguo Li for providing me with this wonderful opportunity. For the past two years, Professor Li has been patiently guiding me and encouraging me to pursue my research. This work heavily relies on his insights and advice.

Besides my supervisor, I would like to thank Professor Fue-Sang Lien and Professor Peter Teertstra for kindly accepting my request to read this thesis.

I would also like to thank every member of Fuel Cell and Green Energy Lab. Without their help I would have not been able to finish this work. I am particularly grateful for the assistance given by our amazing lab manager, Grant Unsworth.

My special thanks are extended to the most awesome office-mates in the world, Andy Shen and Garrett Gauthier, not only for their tremendous help with this work, but also for their friendship throughout my master's program.

I wish to acknowledge the help provided by my friend, Amirali Ashrafizadeh with proof-reading this thesis.

I would like to express my very great appreciation to my family, Fereshteh Tavallari, Mohammad Hossein Roohparvarzadeh, Salar Roohparvarzadeh, Mahboubeh Kangarloo and Mohammad Vakili, and my best friend, Rana Tehrani Yekta, for their endless love, support, and encouragement.

Last but not least, I am forever indebted to my devoted husband, Amirhossein Vakili for his never-ending love, support, understanding, and patience. His continuous help and support made the completion of this thesis possible.

Dedicated to my favourite comedian, Amirhossein Vakili :)

Table of Contents

List of Tables

List of Figures

Chapter 1

Introduction

In today's world, transportation has become a major part of people's daily life. Over the past decades, population growth in Canada has increased the demand for motorized transportation. The dependency of people on road transportation has caused a significant increase in the number of road vehicles [33]. Statistics Canada reported that from year 2000 to 2006, there had been an increase in driving larger and less fuel efficient vehicles, such as vans and pickup trucks [17]. With the increase in the number of road vehicles, especially larger vehicles, air pollution and greenhouse gas emission has become a serious problem. The limited supply of fossil fuel and its environmental impact have increased the need for an alternative power source. One of the most promising candidates for an alternative power source is *fuel cell*. Today, most fuel cells operate using hydrogen fuel, which can be produced from various sources including renewable resources such as biomass, wind, and solar power [62]; as a result, fuel cells not only help with reducing greenhouse gas emission, but also help with reducing world's dependency on fossil fuel.

1.1 Background

A fuel cell, like batteries and combustion engines, is an energy conversion device for power generation. Similar to a battery, a fuel cell is an electrochemical device that converts chemical energy of the reactants to electrical energy [47]. However, unlike a battery, in a fuel cell, the reactants are supplied from an external source and the products are removed from the cell. Thus, a fuel cell has the advantage of continuous operation as long as it is supplied with the reactants and the products are removed from the reaction site.

A fuel cell also offers many advantages over a combustion engine. Since a fuel cell can convert chemical energy directly to electrical, it is more efficient and reliable than a combustion engine. This direct conversion also provides the advantage of making the fuel cell noise and vibration free.

Every fuel cell consists of three active components: an *anode electrode*, a *cathode electrode*, and an *electrolyte* in between the two electrodes [47]. There are many different types of fuel cells that have been developed for numerous applications. Fuel cells can be classified based on various factors, such as their type of electrolyte, their operating temperature, and the type of ion that is transported through the electrolytes. Out of all different types of fuel cells, *proton exchange membrane* or *polymer electrolyte membrane*(PEM) fuel cell is the most ideal for mobile applications. A PEM fuel cell offers many advantages, such as high efficiency even with partial loads, low operating temperature (below 85°C), high power density, and zero emission. However, what makes a PEM fuel cell remarkable is its **solid** polymer electrolyte.

A solid electrolyte allows a simple and compact cell structure, which is insensitive to the orientation [47]. This makes both manufacturing and cell operation of a PEM fuel cell much easier than a fuel cell with a liquid electrolyte. Also, corrosion of cell components is minimal in a PEM fuel cell because there is no free corrosive liquid electrolyte. Less corrosion results in longer cell lifetime. The solid electrolyte can be made very thin (50-200μm) producing a low internal resistance cell, and as a result, high energy efficiency and output power density can be obtained. Another benefit of a solid membrane is its tolerance against large pressure differentials (5MPa) between anode and cathode and pressure fluctuations in the reactant gas supply lines. This helps with avoiding expensive precision sensors and control units.

With all the benefits that a solid electrolyte offers, PEM fuel cells are the most ideal for mobile applications. However, technical challenges and barriers such as cost, durability and performance have been preventing their successful commercialization. Although there has been many progress in research and development towards overcoming these barriers, further improvement is needed before this technology can be widely used [92].

1.2 PEM Fuel Cell

1.2.1 Components of PEM Fuel Cells

The solid electrolyte membrane is the most critical component of the PEM fuel cell. On each side of a membrane there is a cathode or an anode catalyst film where fuel cell

reactions take place [47, 10]. The membrane is sandwiched between two porous transport layers called the *gas diffusion layer* (GDL). The catalyst layer can either be coated on the membrane or on the GDL. These three layers can be hot pressed together into a single piece called *membrane electrode assembly* (MEA), which is the core component of a single cell. MEA is then sandwiched between two flow channels.

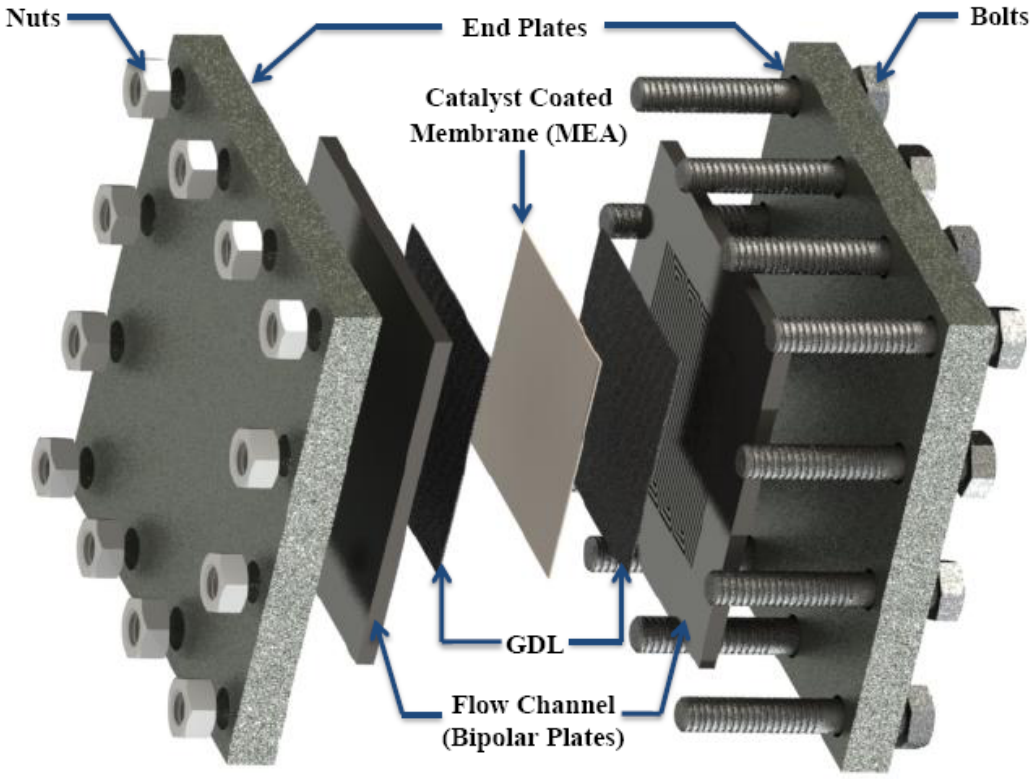

Figure 1.1: Schematic of PEM fuel cell components

To obtain the desirable power output, several single cells can be stacked in series. In a fuel cell stack, MEA is mechanically supported by two electrically conductive plates, called the *bipolar plates*. The role of a bipolar plate is to connect cells electrically in series, separate gases in adjacent cells, provide structural support for the stack, and help the distribution of reactants [11]. Stacks of MEA and bipolar plates are placed between two current collectors and two end-plates. The entire assembly is assembled using nuts and bolts. The components of a single cell assembly is shown in Figure 1.1.

1.2.2 How PEM Fuel Cells Work

To function properly, the proton exchange membrane needs to be fully hydrated. In order to keep the membrane fully hydrated, both the fuel and the oxidants are humidified at 100% relative humidity [47]. Hydrogen is mainly used as the fuel and it is supplied from a flow channel on the anode side. The platinum based catalyst breaks hydrogen into positive hydrogen ions and negatively charged electrons.

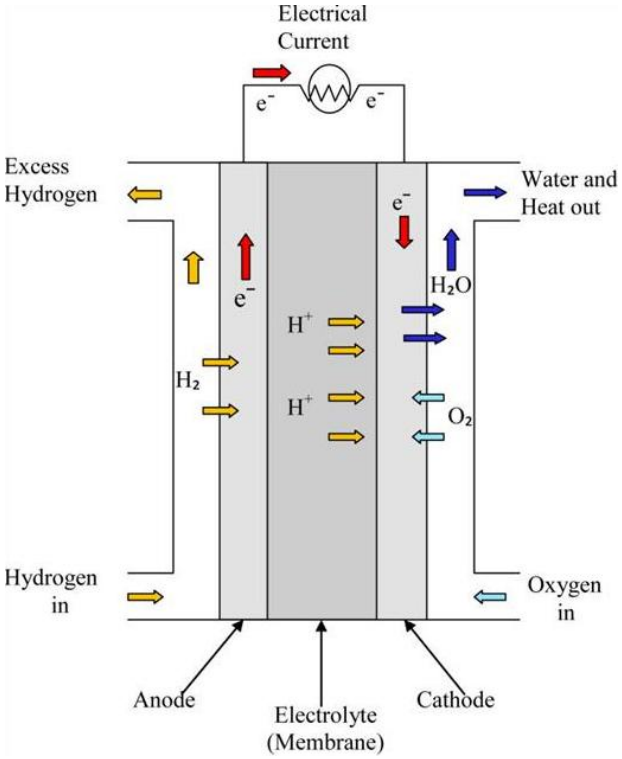

Figure 1.2: Schematic of PEM fuel cell operation [63]

As shown in Figure 1.2, the electrolyte membrane only allows the positively charged ions to pass through, which forces the electrons to travel along an external circuit to cathode, and as a result, an electrical current is created. The reaction at the anode catalyst layer is shown below:

$$H_2 \rightarrow 2H^+ + 2e^- \tag{1.1}$$

On the cathode side, oxygen from air is supplied from the flow channel as the oxidant. Oxygen diffuses through the gas diffusion layer and reaches cathode's catalyst layer. Oxy-

gen molecules react with the electrons and proton (H^+), which have been transferred from the anode, to form water at the catalyst membrane interface. The reaction at cathode catalyst layer is shown below:

$$\frac{1}{2}O_2 + 2H^+ + 2e^- \rightarrow H_2O \tag{1.2}$$

Since the chemical energy stored in hydrogen and oxygen cannot be completely converted into electrical energy, waste heat is also another product of this chemical reaction. Summing up the two reactions at each electrode, the overall cell reaction is:

$$\frac{1}{2}O_2 + 2H_2 \rightarrow H_2O + ElectricalEnergy + WasteHeat \tag{1.3}$$

The produced heat can negatively affect the fuel cell's performance by increasing the average cell temperature and creating temperature gradient throughout the cell. Produced water can also affect the performance by blocking the flow of reactants to reaction sites. Thus, in order for a fuel cell to operate properly, the products need to be effectively removed from the cell. Gas diffusion layer, which is placed next to the catalyst layer, is responsible for helping with water and heat removal from the reaction site.

1.3 Gas Diffusion Layer

Gas Diffusion Layer (GDL) is one of the key components of the PEM fuel cell. This highly porous structure ($\sim 80\%$) is mainly composed of randomly oriented carbon fibres and has a thickness of 100μm to 300μm [47]. GDL is placed between the catalyst layer and the flow channel and it has numerous functions in an operating fuel cell, which includes [65, 57, 29]:

- Removing heat and products from the reaction sight
- Ensuring uniform diffusion of the reactions to the reaction site with minimal pressure drop
- Conducting electrons with low resistance
- Giving physical support to the membrane

GDL can be composed of carbon paper or woven carbon from carbon cloths or woven carbon cloth [55]. Since liquid water is always present in an operating fuel cell, GDL is

typically wet proofed with a *polytetrafluoroethylene* (PTFE) coating to ensure its pores do not become flooded with water. Figure 1.3 shows *scan electron microscopy* (SEM) images of the microstructure of various types of GDLs. As shown in this figure, carbon cloth has a totally different microstructure than carbon paper. Also, carbon paper with PTFE coating looks less porous than carbon paper without PTFE coating.

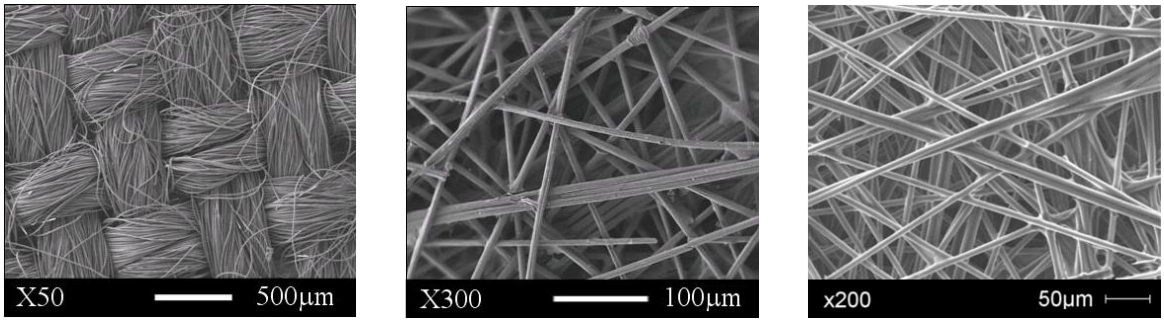

(a) Carbon cloth[79] (b) Carbon paper without PTFE [79] (c) Carbon paper with 5% PTFE [78]

Figure 1.3: SEM images of various types of GDL

Due to the important role that the GDL plays, its volumetric properties, such as porosity, gas permeability, electrical and thermal conductivity, and gas diffusivity can directly affect the performance of the PEM fuel cell [100]. Hence, understanding the physical properties of the GDL is essential for improving the performance of PEM fuel cells. However, the physical properties of the GDL cannot be estimated easily due to its highly porous and random structure; moreover, the GDL can easily be compressed and compression can change its physical properties by breaking and dislocating the carbon fibres. Therefore, physical properties of GDL cannot be correctly estimated without taking the effect of compression into account. Thus, Understanding the compressive behaviour of the GDL is crucial for estimating its physical properties.

1.4 Compression of GDL

In an operating fuel cell, every component, including the GDL, is under compression. Compression changes the microstructure of the GDL and affects its mechanical, electrical and thermal properties, which consequently affects the performance of the PEM fuel cell [42, 29, 48, 25, 18, 100, 101, 97, 64, 19]. The microstructural changes of the GDL

before and after being compressed are shown in Figures 1.4 and 1.5. As seen in these SEM images, the carbon fibres are fragmented and more compact after the GDL has become compressed. Also, the thickness of the GDL is reduced after the compression.

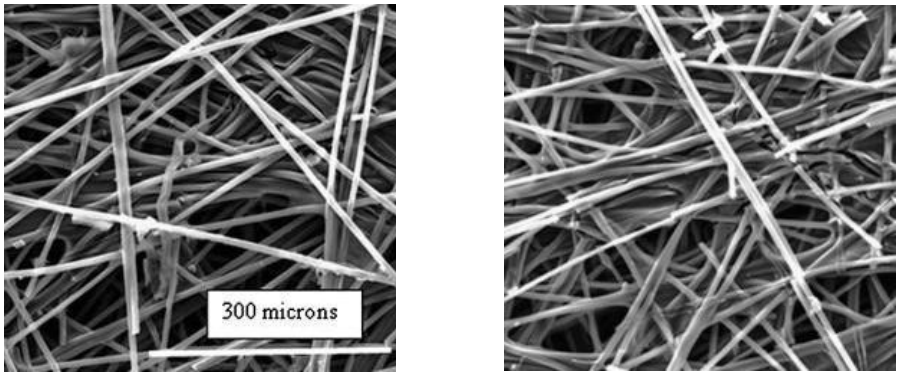

(a) Uncompressed raw GDL (b) Compressed GDL (3.4MPa)

Figure 1.4: SEM images of front surface of raw and compressed GDL [69]

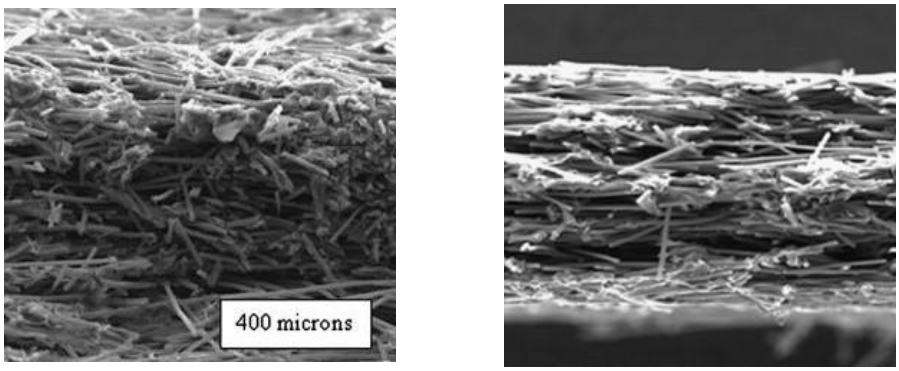

(a) Uncompressed raw GDL (b) Compressed GDL (3.4MPa)

Figure 1.5: SEM images of cross section of raw and compressed GDL [69]

Compressive stresses on the GDL come from two main sources: clamping force of the bolts during assembly and hygro-thermal stresses caused by swelling of the membrane and thermal expansion due to the produced heat from the chemical reactions. Compressive stresses caused by clamping forces have various opposing effects on the performance of the PEM fuel cell. Many studies [60, 58, 61, 94, 2, 73, 39, 54, 34, 38, 43, 93, 102, 5] show that the compression of GDL improves electrical and thermal conductivity by reducing the contact resistance. Thickness change caused by very small compressive loads can also improve gas

diffusivity of reactants and products by shortening the diffusion path [27]. However, too much thickness reduction decreases the porosity of GDL, and as a result, mass transport of reactants and products is reduced; moreover, excessive compressive forces can damage the GDL and reduce the durability of PEM fuel cells.

Temperature and relative humidity variations in a fuel cell cause variation in the applied hygro-thermal stresses. These stresses have a cyclic nature and can also negatively affect the durability and performance of PEM fuel cells.

1.5 Motivation for This Work

Successful commercialization of PEM fuel cells requires major improvements on their performance and durability. To improve the performance of the PEM fuel cell, understanding the mechanical, thermal, and electrical properties of the GDL is critical. These properties are highly affected by the compression of the GDL caused by clamping forces and hygro-thermal stresses. Increase in the compressive forces improves thermal and electrical properties of the GDL. On the other hand, compression negatively affect other physical properties, such as gas permeability and gas diffusivity by decreasing the pore volume. Precise measurements of compressive properties of the GDL can help with estimating GDL's physical properties. Durability of the PEM fuel cell can also be negatively affected by compressive stresses on the GDL. Excessive stresses can change microstructure of the GDL and cause mechanical degradation. Thus, understanding compressive behaviour of the GDL is required for further improvements of PEM fuel cell technology.

1.6 Scope and Outline of The Thesis

In this thesis, the compressive behaviour of the GDL is studied using a new experimental technique. Compressive modulus of the GDL is estimated as a function of temperature, relative humidity, and PTFE content. The effect of cyclic compression on the compressive strain and microstructure of the GDL is also investigated. To better understand the effect of PTFE on the compressive behaviour of the GDL, the pore distribution of GDL samples with various PTFE contents is measured using the method of standard porosimetry.

This thesis is divided into 6 chapters. Chapter 1 gives a brief introduction to PEM fuel cells. In this chapter, the composition and function of the GDL is introduced and effect of compression on properties of the GDL is discussed. In chapter 2, the structural properties

of the GDL are briefly introduced and some basic theories on the deformation of GDL are presented. Chapter 3 is a literature review of various studies on both experimental and numerical prediction of compressive behaviour of the GDL. The experimental method used for estimating the compressive modulus of the GDL under various conditions and its measurement uncertainty is discussed in Chapter 4. The method used for measuring the pore distribution of the GDL is also discussed in this chapter. Chapter 5 presents the results from compression tests and discusses the effects of the factors being studied (temperature, relative humidity, PTFE coating). This chapter also presents and discusses the effects of cyclic loading on compressive strain of the GDL. The last chapter of this thesis contains major conclusions drawn from the results and provides recommendations for future work.

Chapter 2

Structure and Deformation of Gas Diffusion Layer

To understand the effects of compression on physical properties of the gas diffusion layer (GDL), it is best to first learn about GDL's structural properties. In this chapter some basic structural properties of the GDL such as porosity and fibre orientation are introduced. This chapter also briefly introduces some basic concepts such as deformation, stress, and strain and discusses how these concepts are applied in studying the compressive behaviour of the GDL.

2.1 Structural Properties of the GDL

Gas diffusion layer has a highly porous anisotropic structure which does not have a typical behaviour under compressive loads. To understand the compressive behaviour of the GDL, it is better to first learn about some of its structural properties.

2.1.1 Porosity

The most important property of the GDL is its porosity. All other properties of the GDL are directly influenced by the porosity. Porosity is the fraction of the bulk volume occupied by pores in a porous material. The total porosity of a material can be expressed as the following:

$$\phi = \frac{V_p}{V_{total}} \tag{2.1}$$

where ϕ is the porosity, V_p is the pore volume and V_{total} is the total volume of the material. In general, there are three types of pore space: *effective* or interconnected, *isolated* or non-interconnected, and *dead-end* or blind [86]. The effective pore volume is the volume of pore space that is interconnected to both sides of the porous media. The isolated pore volume is the volume of pores that are not connected to any sides of the porous media, and the dead-end pore volume is the volume of pores that are only connected to one side of a porous media. Transportation of matter is then only possible through the effective pore volume.

Porosity of a material can be measured using various experimental methods. The most popular methods include direct method, which measures the bulk volume and then the volume of solid without pores, and imhibition method which fills the pores with a wetting fluid and measures the weight of a sample with and without the fluid and various optical methods [23].

The pore size distribution in a porous material is also very important. Due to the randomness in structure of the GDL, its pore size distribution is not uniform. This makes it very difficult to numerically model the structure of the GDL. The pore size distribution of the GDL can be measured experimentally using various methods such as the method of standard porosimetry [1] and mercury porosimetry [30].

2.1.2 Fibre Orientation and Connection

The mechanical properties of a porous fibrous material are greatly affected by fibre to fibre contact. Mass is transferred through the pores of the GDL while heat and electricity transfer mainly through the carbon fibres and fibre to fibre contact [95]. Thus, the orientation of carbon fibres and how they are connected to each other is very important in determining the thermal and electrical properties of the GDL. The difference in carbon fibre orientation and connection is one of the reasons why carbon paper and carbon cloth with the same porosity have different thermal and electrical properties [91].

Porosity and carbon fibre orientation can both change under an applied compressive load. As the GDL is compressed, the pore volume decreases while the fibre to fibre contact increases. The compressive load also dislocates the carbon fibres and changes their orientation.

2.2 Deformation of GDL

Similar to any deformable solid, GDL's shape and size changes (deforms) under stress. Stress on a body is simply the force applied to that body per unit area [32, 45, 67]:

$$\sigma = \frac{F}{A} \tag{2.2}$$

where σ represents stress, F represents applied force, and A represents the cross-sectional area on which the force is acting on. There are generally two types of stresses: *normal* and *shear*. A Normal stress is caused by a force acting normal to the area while a shear stress is caused by a force acting tangent to the area. Depending on the direction of the force, a normal force can be *tensile* or *compressive*. If the forces are pulling away from an object, then the object is in tension, while if the forces are acting towards an object, the object is said to be under compression. Since in a fuel cell, the forces are acting towards the GDL, compressive stress is of interest for this study.

The most common way to study the deformation of a material is through the stress-strain behaviour of that material. Strain is a measure of the deformation of a body relative to its original shape. Similar to stress, there are two types of strains: *normal* and *shear* [32]. Normal strain is the elongation or contraction along a body per unit length while shear strain is the change in angle of a line along the deformed body. Normal strain is caused by a normal stress and shear strain is caused by a shear stress. Normal compressive strain will be the focus of this study.

The compressive strain can be calculated using Equation 2.3:

$$\varepsilon = \frac{L_0 - L}{L_0} \tag{2.3}$$

where ε is the compressive strain, L_0 is the original length and L is the final length after deformation. According to Hook's law, stress is proportional to strain through the following equation [9]:

$$\sigma = E\varepsilon \tag{2.4}$$

where σ is the stress on the body, ε is the resultant deformation, and E is a constant called the *modulus of elasticity*. Modulus of elasticity can easily be found by performing tension or compression test and plotting tensile or compressive stress as a function of strain. The modulus of elasticity for compression in this study is referred to as the *compressive modulus*. A typical stress-strain curve that can be obtained from a compression test is shown in Figure 2.1. The first region of the stress-strain curve is linear and its slope is the

compressive modulus. In this region the deformation is not permanent and the material will resume its original shape once the applied load is removed. When the stress-strain curve becomes non-linear, the material becomes plastically deformed and will not go back to its original shape. However, as mentioned, the GDL does not have a typical behaviour under stress and may not have an elastic behaviour at all.

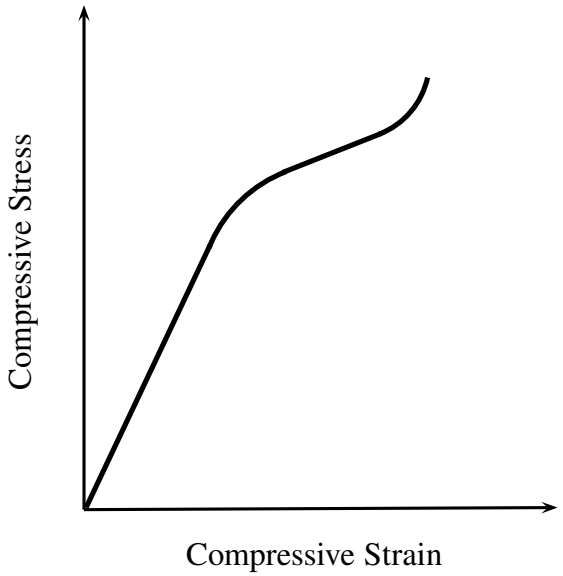

Figure 2.1: Typical compressive stress-strain curve.

In a carbon paper based GDL, which is carbon-carbon composite made out of randomly oriented carbon fibres with diameter of 6μm to 8μm [79, 49], a carbonized matrix holds the fibres together [54]. When the carbon paper is compressed even by a small load, both the matrix and individual fibres can undergo elastic and plastic deformation. Depending on the orientation and structure of the carbon fibre, a carbon fibre composite material undergoes plastic deformation through various failure mechanisms, including [82, 26, 31, 20]:

- fibre bending
- fibre buckling
- fibre kinking
- fibre shear
- fibre crushing

- separation of the fibre from the matrix (fibre-matrix debonding)
- matrix cracking

Even though the overall structure of the GDL is under a compressive load, due to the random orientation of the fibres, each individual fibre can be under shear, tension, or compression and fail differently. Hence, numerical prediction of the compressive behaviour of the GDL by modelling its structure is not very accurate. Although the GDL may not have a typical stress-strain curve, performing compression tests is the best way to take all of the failure mechanisms into account when studying the compressive behaviour of the GDL.

Chapter 3

Literature Review

Due to the porous nature of the GDL, its physical properties can significantly change under compressive load. Therefore, physical properties of the GDL are often estimated as a function of compression pressure. To study the effects of compression on the physical property being estimated, some researchers first measure the thickness change of the GDL under various compressive loads. Thus, the compressive behaviour of the GDL is often not the primary focus of these studies. There are only a few studies that focus strictly on the mechanical properties of the GDL.

3.1 Compression Measurements

A number of researchers have performed compression tests as part of their study on estimating electrical properties of the GDL [58, 25, 56, 53, 41, 70]. Mishra et al. [58], Escribano et al. [25], and Radhakrishnan et al. [70] studied mechanical and electrical properties of the GDL and used similar measurement techniques to estimate the compressive strength of various types of GDLs. Escribano et al. [25] used an INSTRON 4465 mechanical bench with a 5kN load cell to perform two compression tests on each GDL sample. The first considers the effect of pressing used to make the MEA, while the second test shows the effect of compression pressure caused by bipolar plates. They measured thickness changes of various types of GDLs as a function of applied pressure for the range of 0 to 10MPa. They found that the carbon cloth has the highest compressibility and the thickness of both carbon cloth and carbon paper decreases more significantly after the first compression. On the other hand, carbon-felt GDL is less compressive and presents a stable behaviour after

the first test. They also found that samples with PTFE coating are less compressive than the ones without PTFE.

Similarly, Mishra et al. [58] used an INSTRON 5582 universal electromechanical testing system with a 50kN load cell to measure the compressive modulus of various types of GDLs. They divided the compression curves obtained from paper-based GDLs into three piecewise linear regions. They estimated the compressive modulus of GDLs at each of these regions by finding the slope of the line of best fit that goes through each of these three regions. They also found that for a cloth-based GDL, there are actually four linear regions. They presented values for compressive modulus of various types of GDLs for different ranges of compressive stress.

Radhakrishnan et al. [70] studied the difference in structure and properties of carbon paper and carbon cloth. Similar to Mishra et al. [58] and Escribano et al. [25], they used a an INSTRON 3367 test bench in compression mode to study stress-strain behaviour of both carbon paper and carbon cloth based GDLs. To improve accuracy, they stacked 10 samples together. They found that stress-strain curve for carbon paper has two distinct plateaus on the stress-strain curve. The first plateau is caused by compression of stacks causing GDL samples to come closer to each other and reduce the air gap between them. Increase in compression pressure then causes the closure of pores and densifies the GDL, which corresponds to the second plateau. Their results show that carbon cloth is less rigid than the carbon paper and has a non-linear second plateau as opposed to carbon paper which has an almost linear second plateau.

To study the electrical contact resistance between a metallic bipolar plate and the GDL, Matsuura et al. [56] first evaluated the compressive characteristics of the GDL by performing compression tests at room temperature. They measured compressive stress-strain relation of carbon-paper-based GDL (TGP-H-090) for compression pressure of up to 20MPa. They found that the compression rigidity of the GDL remains constant for up to 15MPa, but as the pores of the GDL get destroyed, the compression rigidity suddenly increases.

Mason et al. also studied the effect of clamping pressure on mechanical and electrical properties of the GDL [53]. They conducted experiments using a commercially available cell compression unit (CCU)(Pragma Industries SAS), which allowed controlled compression of the GDL sample between two flow field plates while measuring thickness change with a resolution of $\pm 1\mu$m for loading compression pressure of up to 2.5MPa and unloading compression pressure of 0.2MPa. They found that after compressing the GDL by 2.5MPa, the GDL exhibits irreversible compression, which changes its original thickness by 32% after unloading.

Kleeman et al. studied local compression distribution in the GDL and examined its effects on the electrical resistance [41]. To study the relation between stresses applied externally and strains occurring inside the GDL, they applied finite element method (FEM) with detailed material characterization. Using Hook's law, they developed a macroscopic structural material model based on the assumption of orthotropic mechanical behaviour for fibrous paper and non-woven GDL:

$$\begin{bmatrix} \sigma_x \\ \\ \sigma_y \\ \\ \tau_{xy} \end{bmatrix} = \begin{bmatrix} \dfrac{E_x}{1-\nu_{xy}\nu_{yx}} & \dfrac{\nu_{xy}E_y}{1-\nu_{xy}\nu_{yx}} & 0 \\ \\ \dfrac{\nu_{xy}E_y}{1-\nu_{xy}\nu_{yx}} & \dfrac{E_y}{1-\nu_{xy}\nu_{yx}} & 0 \\ \\ 0 & 0 & G_{yx} \end{bmatrix} \begin{bmatrix} \varepsilon_x \\ \\ \varepsilon_y \\ \\ 2\varepsilon_{xy} \end{bmatrix} \tag{3.1}$$

where E_x is Young's modulus or modulus of elasticity in the material plane, E_y is Young's modulus through the material plane, ν_{xy} is the Poison's ratio, and G_{xy} is the shear modulus. To solve the equations above, they conducted experiments to measure the materials' properties. To find E_y, they performed compressive tests on GDL samples using a material tester (Zwick-Roell, type Zwicki). Original thickness of each sample was measured using three high-resolution inductive distance sensors that were fixed to the device. They measured thickness of compressed samples for compression pressure of up to 1.8 MPa and found that every sample has a non-linear declining compressive behaviour with pronounced material hardening at high strains. They also found that E_y has to be expressed as a function of compression itself and the particular value for E_y at a certain compression has to be calculated using a secant modulus $E_{y,1}$:

$$E_{y,1} = \frac{\sigma_{y,1}}{\varepsilon_{y,1}} \tag{3.2}$$

where $\sigma_{y,1}$ and $\varepsilon_{y,1}$ are applied force and ratio of thickness change to initial thickness respectively. A polynomial curve fit was used to express E_y as a function of strain and then used as an input for the structural simulation.

Yi et al. used numerical modelling to estimate elastic properties of a unidirectional GDL and validated their results by conducting uniaxial tensile and compression tests [96]. They used a micromechanical model for porous material developed by Zhao et al. [99] and assumed carbon paper is macroscopically homogeneous and transversely isotropic. They calculated five independent elastic constants for the unidirectional carbon paper, including

in-plane tensile moduli and out-plane compression modulus. They also measured thickness changes of the GDL as a function of compressive load using an optical microscope and found that stress-strain curves for both tension and compression tests were non-linear. They also found that in-plane tensile moduli is much higher than out-of-plane compression modulus. They used a least square linear regression to obtain elastic moduli of the GDL. The estimated numerical values of elastic moduli were in less than 20% discrepancy of values obtained from tension and compression tests.

Nitta et al. [60, 94], Sadeghi et al. [73], Sadeghifar et al. [74] and Unswroth et al. [88] all studied thermal properties of the GDL as a function of compression pressure. Nitta etl al. performed compressive tests on GDL samples (SGL SIGRACET 10BA) by compressing the sample with a steel rod that was loaded with weight. They measured the thickness using a dial indicator. Since the GDL is easily deformed at a very low pressures, they performed additional measurements at pressure lower than 0.1MPa. The original thickness of the samples were estimated using measurements with a low compression pressure. They performed measurements on stacks of 1-4 GDLs and found that the most noticeable variation in GDL's strain is at low pressures, approximately below 0.2MP. Stress-stain curves for different number of GDLs indicated almost identical behaviour with smaller strains for stacks with higher number of GDL samples.

Sadeghifar et al. [74] studied the effect of PTFE content and micro porous layer on thermal conductivity of the GDL. They measured the thickness change of GDL samples (SGL 24AA, 24BA, 24DA, 24DC, 25AA, 25BA, and 25BC) with different PTFE content as a function of compression pressure and found that every curve has a non-linear, almost exponential behaviour for pressures below 7 bar. The thickness reduction in this region is steep. However, for pressure range of 7 to 15 bar, the thickness reduction becomes shallower and varies linearly with pressure. Although all of the samples showed a similar trend, the samples with PTFE coating had less thickness reduction. The thickness reduction trend found in this study is consistent with results found by other researchers [39, 8, 60].

Unsworth et al.[88] studied the effects of compression on thermal conductivity of SolviCore GDLs . They also measured the thickness of GDL samples as a function of compression pressure. Unlike other studies, they found that the thickness of SolviCore GDL changes linearly with applied pressure for compression pressures of up to 15 bar.

Sadeghi et al. [73] also studied the effect of compressive load on thermal conductivity of GDL. They used a tensile-compressive apparatus to measure the GDL's thickness variation at various compressive loads. They measured the thickness using Mitutoyo digital indicator with 0.001mm resolution while the samples were compressed by a steel rod using a pneumatic actuator. The compression pressure was measured using a load cell with 2.5%

accuracy. They found that the carbon paper deforms non-linearly with pressure. They used an exponential correlation to describe compressive strain of the GDL as a function of compressive stress. This correlation was then used in their analytical model to estimate the thermal conductivity of the GDL.

Ismail et al. [37] investigated the mechanical behaviour of a number of GDL samples and sealing gasket under compression. Unlike other studies, this study is strictly focused on the compressibility of the GDL. They particularly investigated the effect of PTFE coating and the presence of sealing gaskets on compressive behaviour of the GDL. Ismail et al. performed compression tests on SGL GDL samples using an INSTRON 5566 universal testing machine with a 10kN load cell. The initial thickness of the sample was measured by measuring the displacement of a compression plate with and without the sample. The test results were presented as compressive stress-strain curves. They found that for every compression curve, there are three distinctive regions. In the first region, which only covers compression pressures of 0 to 0.01MPa, the compressive strain increases linearly and rapidly with compressive stress. In the second region, which starts at compression pressure of 0.01MPa and ends at 1MPa, the strain increases non-linearly and slowly with increase in stress. Stress-strain behaviour of the GDL becomes linear again for compression pressure higher than 1MPa, but in this last region the strain increases much slower than the first region. Since the GDL normally compressed by a compressive stress of 1MPa to 1.4 MPa, the last region is the region of interest for PEM fuel cells. Study on PTFE coating showed that higher PTFE loading makes the GDL stiffer and less compressible. This has to to do with the fact that PTFE coating decreases the porosity of the GDL, which consequently makes it more compact and less compressible. The experiments that were performed on sealing gasket showed that a gasket is far less compressible than the GDL. They also performed compression tests on combined stacks of GDL and gasket samples. They found that a fourth order polynomial curve fits their data perfectly. All their data was corrected for machine compliance by subtracting the deformation of a machine from their results. This was done by running the experiment without a sample and measuring the thickness change of the machine as a function of compressive load.

Lai et al. [44] studied the local compressibility of the Toray paper GDL using a numerical model. They also validated their results by performing platen compression test. They found that even small thickness variation throughout the GDL can cause local compression pressure of up to 3MPa for an applied pressure of 1.4MPa.

To study the microstructure of a compressed GDL, a few researchers [56, 13, 69, 83, 81, 25] have compared SEM images of compressed and uncompressed GDL samples. Although this method helps with understanding the effect of compression on microstructure of the GDL, it does not provide any quantitative results, which could be used for estimating other

physical properties of the GDL.

Even though the compressive behaviour of the GDL has been studied by many researchers, there is no current study that takes the effects of the PEM fuel cell operating parameters, such as temperature and relative humidity into account. As shown in Table 3.1, a PEM fuel cell typically operates at temperatures above 60°C and relative humidity of near 100%. These conditions may affect the compressive behaviour of the GDL and their effects should be investigated.

Table 3.1: Typical Operating Conditions of polymer electrolyte membrane fuel cell [12, 28]

Typical Operating Condition	
Temperature	60°C - 90°C
Pressure	1.2 - 1.5 MPa
Relative Humidity of Reactants	60% - 100%

As mentioned earlier, the physical properties of the GDL cannot be estimated without the knowledge of GDL's elastic/plastic properties. Estimating the compressive modulus of the GDL can be useful for many researchers that study the thermal and electrical properties of the GDL. Most of the studies that were mentioned above do not provide an estimated value for the compressive modulus.

3.2 Cyclic Compression

In a fuel cell environment, changes in relative humidity and temperature cause a variation in the resultant hygro-thermal stresses. The changes in applied stresses can have a cyclic effect. A few researchers who have studied the compressive behaviour of the GDL have also performed experiments to study the effects of cyclic loading on the thickness reduction of the GDL.

To investigate the effect of cyclic loading, Sadeghi et al. [72] used the same tensile-compression apparatus that was used for performing compression tests in their previous study [73]. They performed cyclic compression experiments by loading and unloading GDL samples at various compressive loads. They recorded the pressure and thickness of the sample while loading and unloading until there was no significant hysteresis effects in the loading-unloading curves. This was found to occur after the 5th cycle. Their results showed that the thickness reduction is more significant at the beginning of the loading and

as the compression pressure increases, the thickness variation decreases. The thickness of the GDL samples changed by 4.5% after the first loading-unloading cycle. The thickness variation increased to 7% after 5 cycles and remained unchanged afterwards. Stankovic et al. [80] also found similar behaviour for various types of fibrous materials.

Radhakarishnan et al. [69] investigated the effect of cyclic compression on structure and properties of GDLs. They simulated repeated opening and closing of fuel cell hardware by subjecting Toray paper GDL samples to five cycles of compression. They found that cyclic compression causes irreversible changes to the structure and properties of the GDL including surface morphology, surface roughness, pore size, void fraction, thickness, and electrical resistance. The effect of cyclic compression on residual strain of the GDL samples was found to be significant and progressive. Their results show that the thickness reduction of sample increases with every compression cycle. This is inconsistent with what was found by Sadeghi et al. [72].

Mathias et al. [54] characterized the compressive properties of the GDL by placing a stack of GDL samples between two flat plates and measuring the deflection as a function of compressive force. They loaded both carbon paper and carbon cloths GDL samples by a pressure of up to 2.75MPa and then decreased the load to zero for 10 repeated cycles. The first cycle had a different behaviour than the other cycles, suggesting that the material weakens once it is under pressure for the first time. They also found carbon cloth to be more compressive than carbon paper, but found carbon paper to be more elastic than carbon cloth.

All of these studies suggest that compressive load changes the microstructure of the GDL. Thus, it has a different behaviour every time that it gets compressed. These studies only show the effects of cyclic compression for at most 10 cycles. However, every time the fuel cell starts up or shuts down the compressive load on the GDL changes. For automotive applications, a PEM fuel cell is estimated to undergo about 30,000 start-up/shut-down cycles [7]. Thus, to improve the durability of the GDL, cyclic loading test should be performed for a much higher number of cycles.

3.3 Summary

Although a lot of effort has been put into understanding the mechanical behaviour of GDLs, there still is not any study that focuses on parameters such as temperature and relative humidity. Also, the effect of fatigue has not yet been studied. Most studies on cyclic loading only consider 10 cycles at most. However, a GDL that is used for automotive applications

Table 3.2: Summary of the literature review on compressibility of GDLs

Author	Method Used	Compressive Modulus	Effect of PTFE	Effect of Temp	Effect of RH
Chang et al. [18]	Experimental	No	No	No	No
Escribano et al. [25]	INSTRON 4465	Yes	No	No	No
Ismail et al. [37]	INSTRON 5566	Yes	Yes	No	No
Kleeman et al. [41]	Experimental	No	No	No	No
Lai et al. [44]	Experimental and numerical	No	No	No	No
Mason et al. [53]	Fuel cell compression unit	No	No	No	No
Matsuura et al. [56]	Experimental	No	No	No	No
Mishra et al. [58]	INSTRON 5582	Yes	Yes	No	No
Nitta et al. [60]	Experimental	No	No	No	No
Radhakrishnan et al. [70]	INSTRON 3367	No	No	No	No
Sadeghi et al. [73]	Tensile/compressive apparatus	Yes	No	No	No
Sadeghifar et al. [74]	Experimental	No	Yes	No	No
Unsworth et al. [88]	Experimental	No	No	No	No
Yi et al. [96]	Experimental and numerical	Yes	No	No	No

should undergo 30,000 cycles. Table 3.2 summarizes the studies found in literature that investigated the compressive behaviour of the GDL using experimental measurements or numerical modelling. As shown in this table, none of these authors have considered the effects of relative humidity or temperature. Also, most of the authors have not provided an estimated value for the compressive modulus.

Chapter 4

Experimental Setup

This chapter explains the methods that are used for compression tests and cyclic compression tests. Data analysis and measurement uncertainty for the compression test is also explained in this chapter. The last section of this chapter explains the standard method of porosimetry that is used for finding the pore size distribution of the GDL.

4.1 Compression Test

To measure and characterize the compressive behaviour of the GDL, a compression measurement apparatus is used. This apparatus was originally designed for thermal conductivity measurements and measures the total thermal resistance of a sample as a function of applied compressive load. To do that, the sample is compressed by a controlled compressive load. This apparatus also measures the thickness of the compressed sample with high accuracy. Thus, with a few modifications, this apparatus can easily be used for measuring the thickness of the sample as a function of applied compressive load while having the benefit of controlling the temperature of the sample during the compression test.

4.1.1 Original Testing Apparatus

The compression apparatus used for compression measurements was originally a thermal conductivity apparatus that was used by Unsworth et al. [88, 87]. This apparatus is an evolution of previous design by Culham etl al. [21] and follows the measurement technique described in the ASTM standard D 5470-06 [46]. This experimental method is a steady-state

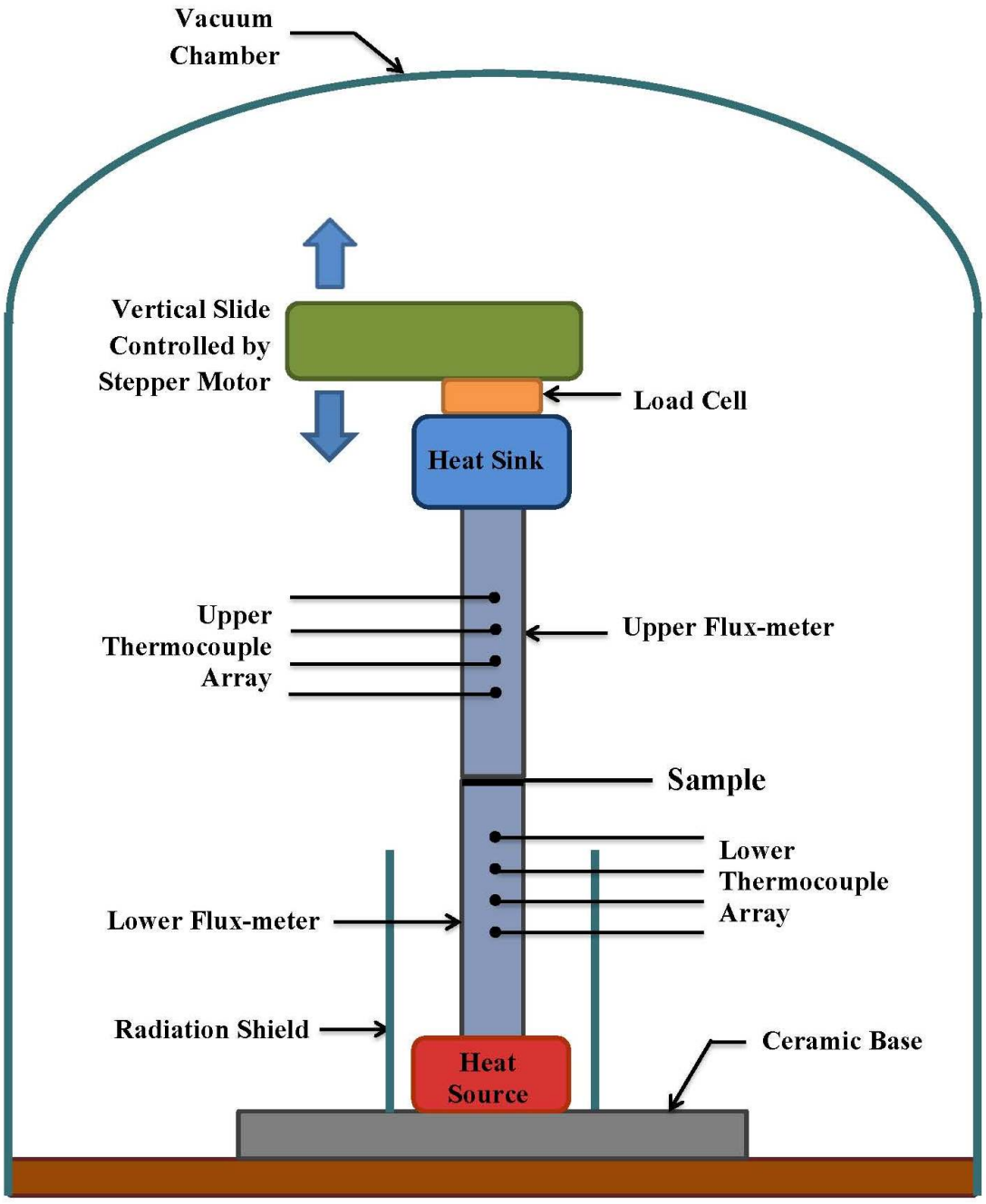

Figure 4.1: Schematics of the original testing apparatus that was used for thermal conductivity measurements

approach which uses guarded one-dimensional heat flow to measure thermal conductivity of thin films and is very popular amongst many researchers [60, 39, 73, 72, 15, 40, 71, 16].

In the original design, this apparatus was used to measure the total thermal resistance of a sample by creating a one-dimensional heat flow through the sample [87]. Figure 4.1 shows the schematic of the thermal conductivity apparatus before being modified. As shown in Figure 4.1, the sample is compressed between two calibrated rods, called flux-meters. The flux-meters are made out of electrolytic iron, which has a calibrated thermal conductivity that maximizes the temperature drop across the sample. The bottom of the lower flux-meter is heated using an electric heater and the top of the upper flux-meter is cooled by circulating water from a constant temperature bath. The temperature gradient along each flux-meter is measured using 4 equally distanced k-type thermocouples. The temperature of the sample can be estimated by extrapolating the temperature gradient measured by the thermocouples. To ensure one dimensional heat flow, the thermal conductivity apparatus is placed in a vacuum chamber to prevent convective heat transfer, and a radiation shield is placed around the lower flux-meter to minimize heat transfer through radiation.

The lower flux-meter is fixed to a ceramic base with low thermal conductivity, while the upper flux-meter is attached to a vertical slide, which is controlled by a Velmex stepper motor [87]. The stepper motor can apply compressive stress of up to 1.5MPa for a sample with 3/4 inch diameter. The stepper motor also measures the sample's thickness by first recording the position of the top flux-meter at the desired compression pressure without the sample, and then recording the position at the desired compression pressure with the sample.

The applied force is measured using a Honeywell Sensotec load cell. To minimize the effect of thermal expansion, the upper and lower flux-meters are set to be in contact without the sample until the desired temperature is reached. After this warm up period, the position of upper flux-meter is recorded at the desired compression pressure without the sample. After placing sample on the lower flux-meter, the test starts by compressing the sample to the desired compression pressure. To ensure that a steady-state is reached, the sample stays compressed between the two flux-meters for about one hour. A data acquisition system records the position of the flux-meter, the temperature of each thermocouple and the force applied by the stepper motor once the steady-state is reached. This procedure can then be repeated for various compressive loads.

4.1.2 Modified Testing Apparatus

At room temperature, the thickness change of the GDL sample can easily be measured as a function of compression pressure without making any modification to the previous design. Measurements at room temperature are done by shutting both the electric heater and the temperature bath off so that flux-meters are both kept at room temperature. The vacuum chamber and radiation shield are not used since creating a 1-dimensional heat flow is not required for this type of experiment. Also, since the sample does not need to reach steady-state for compressive measurements, the thickness and compressive force can be recorded as soon as the desired compressive force is reached. The sample is subjected to a range of compressive loads starting at approximately 2N and increasing to approximately 440N in about 50 measurement steps. Depending on the size of the sample, the applied forces can correspond to different compressive stresses.

For the results to be accurate, the compressive force should be applied perfectly normal to the surface of the GDL and the stress should be distributed evenly throughout the surface of the sample. To ensure that the compression apparatus applies a uniform compressive stress, a pressure indicating film is used to reveal the pressure distribution on a compressed GDL. Pressure indicating films used at compression pressures of 1.7MPa and 3.4MPa are shown in Figures 4.3a and 4.3b respectively. It can clearly be seen that the colour intensity is fairly uniform for both tested pressures.

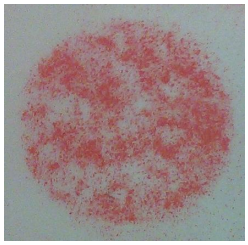

(a) Pressure indicating film for sample at 1.7MPa

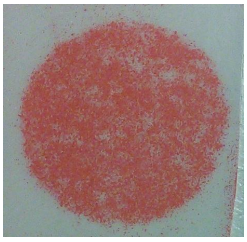

(b) Pressure indicating film for sample at 3.4MPa

Figure 4.3: The pressure distribution on compressed GDL samples at pressures of 1.7MPa and 3.4MPa on pressure indicating film

To study the effect of temperature and relative humidity, the apparatus was modified mainly by adding an environmental chamber. The schematic of the modified apparatus is shown in Figure 4.2. To keep the sample at a desired temperature and relative humidity, air with controlled temperature and relative humidity is supplied from a fuel cell test station

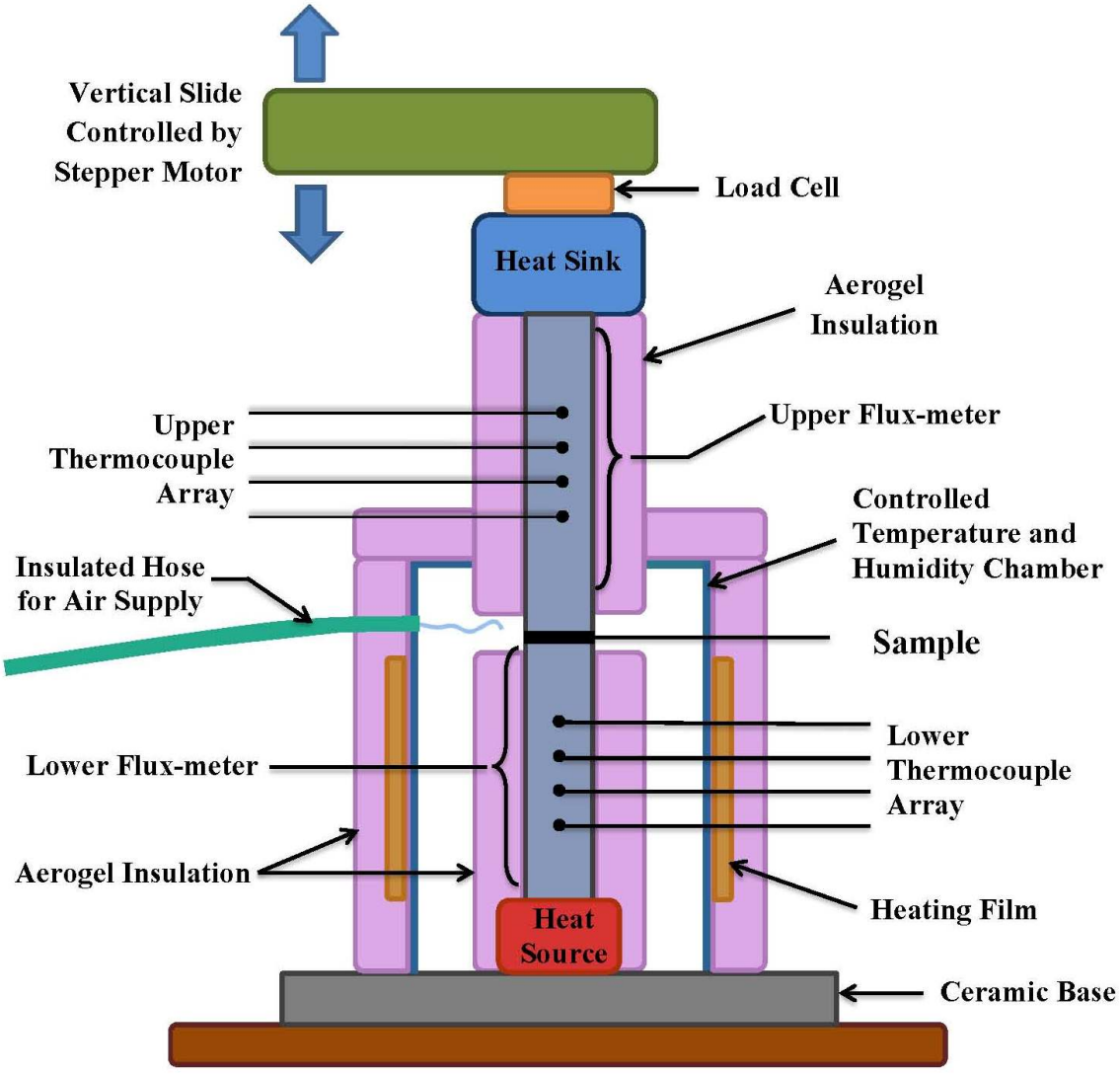

Figure 4.2: Schematic of the modified testing apparatus that is used for compression tests

to the chamber through an insulated plastic hose. The chamber is made out of aluminium, which is excellent heat conductor. This ensures that the temperature of the air inside the chamber is uniform. On the other hand, high thermal conductivity will increase the heat loss to the surrounding environment. This can particularly cause problems with excessive condensation that forms while testing GDL samples at high relative humidities. To avoid heat loss and condensation, the chamber is heated by a heating tape and is then insulated with Pyrogel XT-E. Pyrogel XT-E is a hydrophobic flexible thermal insulator made out of silica aerogel, which can be used for high temperature applications. It's hydrophobic nature makes it an excellent insulator to be used for insulating the upper and lower flux-meters. Physical properties of Pyrogel XT-E are shown in table 4.1.

Table 4.1: Physical properties of Pyrogel XT-E [35]

Physical Property	
Thickness	5 mm
Density	0.2 g/cc
Maximum Temperature Use	650°C
Thermal Conductivity at 100°C	0.023 W/mK

To maintain a uniform temperature across the sample, both the thermal bath and the electric heater are set to have the same temperature. Two to three hours before the start of a test, samples are placed inside the chamber to become exposed to the desired testing temperature and relative humidity. To ensure that a sample is at the desired temperature and relative humidity, the compressive force and thickness measurements are recorded after the sample has been kept at the desired compressive load for at least five minutes.

Each test is repeated 10 to 15 times to obtain a meaningful statistical analysis. Since the GDL's microstructure changes when it is subjected to a compressive load, for each repeated test new samples are used.

4.1.3 Test Samples

Two different types of GDL from different manufacturers are used in this study: SpectraCarb 2050A-0850 carbon paper and Toray Paper TGP-H-120. SpectraCarb 2050A carbon paper is used for studying the effect of temperature and relative humidity. The manufacturer's specifications for this untreated carbon paper is shown in Table 4.2. To study the effect of PTFE coating, Toray paper with different PTFE loadings (0%, 5%,

10%, 20%, 30% and 40%) is used. The specifications given by the manufacturer for Toray paper TGP-H-120 are shown in Table 4.3.

Table 4.2: Physical properties of SpectraCarb 205A-0850 carbon paper given by the manufacturer [50]

Physical Properties	
Thickness	0.203 mm
Compressive Strength	2.1 MPa
Flexural Strength	37 MPa
PTFE Coating	No

To increase the maximum compressive stress that can be applied to a sample, the GDL samples are cut in smaller disks with 1/2 inch diameter, instead of 3/4 inch. This results in a maximum compression pressure of 3.5MPa. As shown in Table 4.2, compressive strength of SpectraCarb carbon paper provided by the manufacturer is 2.1MPa. The operating compressive stress in a PEM fuel cell is approximately between 1MPa to 1.4MPa [58, 18, 22, 98]. Therefore, a maximum compressive stress of 3.5MPa is adequate for the purpose of this study.

To reduce thickness measurement errors, depending on the type of the test and the sample type, samples are tested in stacks of four to six. For compression tests at high temperature or high relative humidity, stacks of four samples are tested, while for tests at room temperature, stacks of 6 samples are used for SpectraCarb paper and stacks of four samples are used for the Toray paper.

Table 4.3: Physical properties of TGP-H-120 carbon paper given by the manufacturer [51]

Physical Properties	
Thickness	0.37 mm
Porosity	78%
Flexural Strength	40 MPa
Tensile Strength	90 MPa

4.1.4 Data Analysis

To obtain a compressive stress-strain curve, stress and strain are calculated using the parameters measured by the compressive apparatus. The compressive stress is calculated using the measured compressive force and the cross-sectional area of the GDL sample:

$$\sigma_{comp} = \frac{F_{comp}}{A} \tag{4.1}$$

where σ_{comp} is the compressive stress, F_{comp} is the compressive force measured by the load cell and A is the cross-sectional area of a sample. The compressive strain is calculated using sample's original thickness and the thickness measured at each compressive load:

$$\varepsilon_{comp} = \frac{t_o - t}{t_o} \tag{4.2}$$

where ε_{comp} is the compressive strain, and t_o and t represent the original thickness and the measured thickness at specific compressive load respectively. Sample's original thickness is estimated by measuring the thickness at a very small compression pressure and then extrapolating the original thickness at zero compression pressure.

4.1.5 Measurement Uncertainty

Similar to any experiment, this experimental setup also has two main sources of error: bias and precision [84]. The total measurement uncertainty is the summation of both bias and precision error:

$$u = \sqrt{b^2 + p^2} \tag{4.3}$$

where u stands for uncertainty, b for bias error, and p for precision error. To take the effect of precision error into account, the standard deviation of both stress and strain are calculated for series of repeated measurements.

Since stress is a function of the applied force and the cross-sectional area, the measurement bias of stress depends on the accuracy of these two parameters. The load cell that measures the force has an accuracy of $\pm 1\%$ of the measured force. The uncertainty in the calculated area of the sample mainly comes from misalignment of the stacked sample and is estimated to be $\pm 5\%$ of the total area. Using Equation 4.1, the overall bias error for

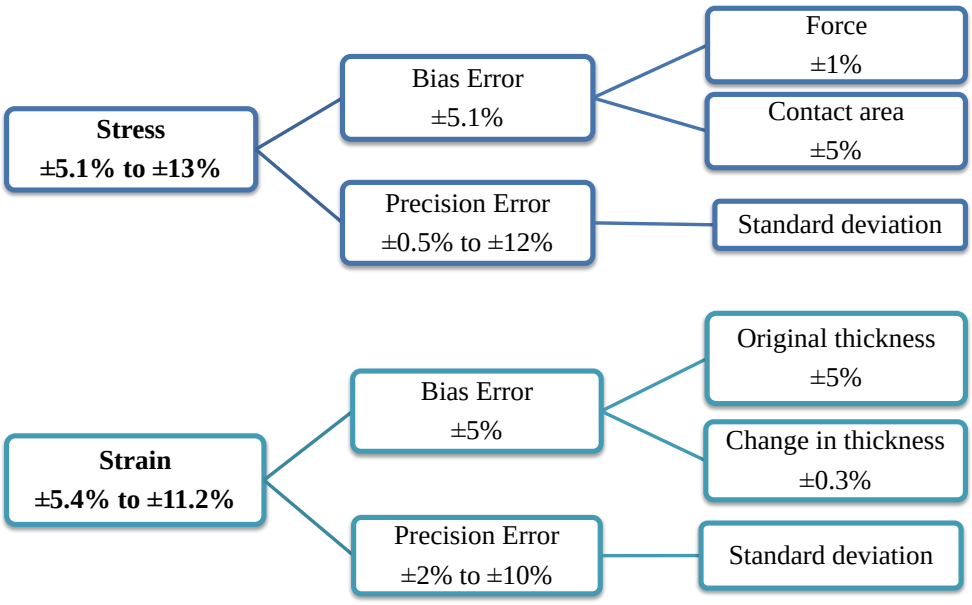

Figure 4.4: Error analysis performed for compression measurements

calculated stress can be estimated as follow [85]:

$$\frac{\delta\sigma}{\sigma} = \sqrt{\left(\frac{\delta F}{F}\right)^2 + \left(\frac{\delta A}{A}\right)^2} \tag{4.4}$$

The total bias error for stress measurement obtained from Equation 4.4 is ±5.1%.

The bias in calculated value of strain comes from uncertainty in measuring the original thickness and the final thickness. Since the stepper motor measures the thickness at 1.5μm per step, it has an accuracy of ±1.5μm. For a stack of 4 compressed sample with thickness of approximately 500μm, the measurement error can be estimated using Equation 4.5:

$$\frac{\delta t}{t} = \frac{1.5\mu m}{500\mu m} = \pm 0.003 \tag{4.5}$$

Since the original thickness is estimated using a very low pressure, the uncertainty in measuring the original thickness is larger than the value calculated above. The uncertainty in measuring the original thickness is then estimated to be 40μm. For a typical stack of four samples with original thickness of about 800μm, the measurement uncertainty is estimated

as shown below:

$$\frac{\delta t_o}{t_o} = \frac{40\mu m}{800\mu m} = \pm 0.05 \tag{4.6}$$

The overall bias in the calculated value of strain is found using Equation 4.7:

$$\frac{\delta \varepsilon}{\varepsilon} = \sqrt{\left(\frac{\delta t_o}{t_o}\right)^2 + \left(\frac{\delta t}{t}\right)^2} \tag{4.7}$$

The total bias error for a typical calculated strain value is found to be ±5%. The uncertainty analysis performed for compression measurements is summarized in Figure 4.4.

4.2 Cyclic Compression Measurements

The compression apparatus used for compression measurements is also used for cyclic compression tests with modified LabVIEW programming code. To simulate the cyclic pressure that the GDL undergoes during fuel cell operation, the sample is compressed by a compression pressure of 2MPa. Once the compression pressure reaches 2MPa, the thickness of the sample is measured and the apparatus starts to unload until the compression pressure reaches 1MPa. This pressure simulates the clamping pressure that the GDL experiences in an assembled fuel cell when the fuel cell is not operating. This loading and unloading cycle is then repeated as many times as required to simulate the effects of start-up and shut-down of a PEM fuel cell. The thickness of the sample is measured only at compression pressure of 2MPa at every cycle. The strain at each cycle is calculated as explained in Section 4.1.4.

To further investigate the effect of unloading on stress-strain behaviour of the GDL, the thickness of a stack of 8 samples is measured during loading and unloading for 7 repeated cycles. Stress-strain curves for all of the loading/unloading cycles are obtained by analyzing the measured values as explained in Section 4.1.4.

Both of these experiments are performed using untreated SpectraCarb-2050A carbon paper GDL.

4.3 Porosity

To better understand the effect of PTFE coating on stress-strain behaviour of the GDL, the pore size distribution of samples with various PTFE contents are measured. To measure the pore size distribution, the method of standard porosimetry (MSP) is used. The MSP apparatus that is used for measuring the pore size distribution in this study is built by Greenlight Innovations (Burnabay, British Columbia) [36].

4.3.1 Standard Porosimetry Measurement Principle

The method of standard porosimetry is based on the law of capillary equilibrium [90]. According to this law, if two or more porous bodies are filled with a wetting liquid and are at capillary equilibrium, then the capillary potentials for each of these porous bodies are equal:

$$\psi_1 = \psi_2 = ... = \psi_i = \psi \tag{4.8}$$

where ψ_1, ψ_2, and ψ_i are the capillary potential for first, second and the ith porous body respectively.

This method relates the volume of the liquid in a porous sample with unknown porosity to the volume of the liquid in a calibrated standard porous sample with known porosity and pore size distribution:

$$V_t = f_t(V_s) \tag{4.9}$$

where V_t is the volume of the liquid in the test sample and $f_t(V_s)$ is the function that relates the volume of the liquid in the test sample to the volume of the liquid in the calibrated standard sample.

The integral liquid distribution of the calibrated standard sample as a function of capillary potential is known and provided by the manufacturer:

$$V_s = f_s(\psi) \tag{4.10}$$

where V_s is the liquid volume in standard sample and $f_s(\psi)$ is the function relating the distribution of liquid in standard sample to the capillary potential.

Using Equations 4.8, 4.9, and 4.10, the volume of the liquid in the test sample can be written as a function of capillary potential:

$$V_t = f_t[f_s(\psi)] \tag{4.11}$$

Once the standard sample and the test sample are in contact, the capillary equilibrium is reached by the flow of liquid and vapour, which is caused by gradients in capillary potentials. The capillary potentials are formed by the capillary pressure P_c, which is a function of vapour pressure of the liquid (P_v) and the saturated vapour pressure (P_s):

$$P_c = \frac{P_v}{P_s} \tag{4.12}$$

The capillary pressure can then be related to the maximum radius of pores filled with liquid using Laplace equation:

$$P_c = -\frac{2\gamma cos\theta}{r_m} \tag{4.13}$$

where γ is the surface tension of the wetting liquid, θ is the wetting angle, and r_m is the maximum radius of pores filled with liquid. To find the relation between the volume of liquid in a test sample and the volume of liquid in a calibrated standard sample, the weight of each sample is measured at various liquid saturations while letting the liquid in both samples to evaporate over time.

A radial pore distribution function is then derived by equating the value of P_c to capillary potential and combining Equations 4.11 and 4.13:

$$V_t = f_t \left[f_s \left(-\frac{2\gamma cos\theta}{r_m} \right) \right] \equiv F(r) \tag{4.14}$$

where r is the radius of the pore.

Using octane as the wetting liquid with $\theta \sim 0$, Equation 4.14 can be simplified:

$$F(r) \equiv f_t \left[f_s \left(\frac{-2\gamma}{r} \right) \right] \tag{4.15}$$

To better understand how the MSP works, a typical pore size distribution curve for a porous body obtained from the MSP is shown in Figure 4.5 [90, 1]. Three curves are seen in this figure:

1. The pore size distribution provided by the manufacturer for the standard sample shown on the right side of the plot. This curve plots the volume of liquid in standard sample (y-axis) as a function of pore radius (x-axis).

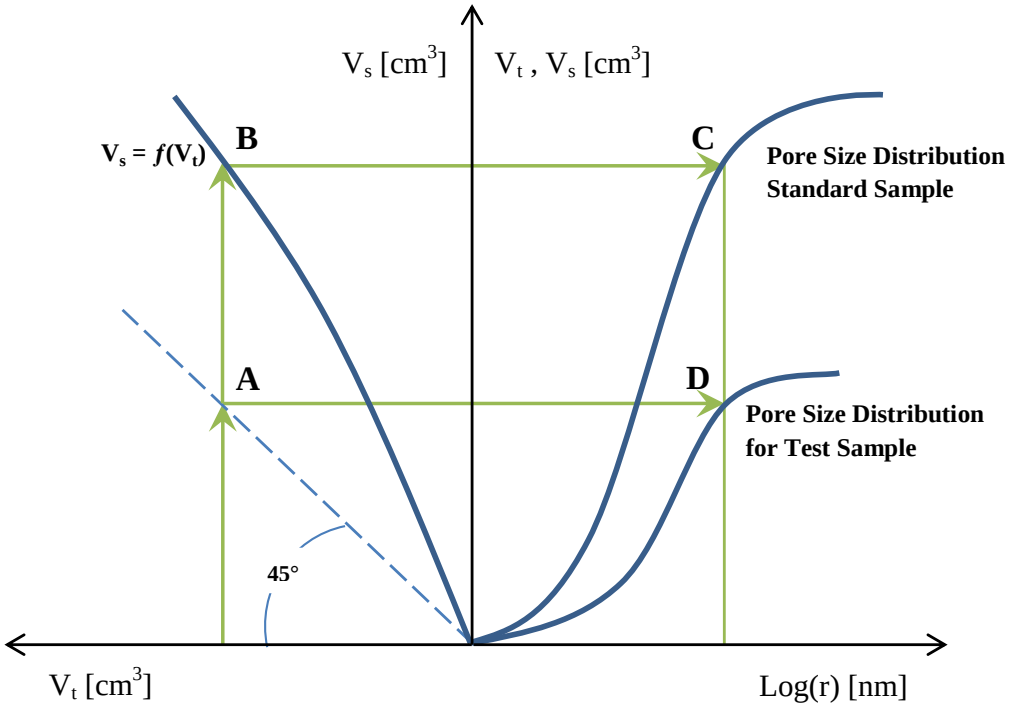

Figure 4.5: Typical plot for measuring pore size distribution of a porous media using the method of standard porosimetry [90, 1]

2. The curve shown on the left side, which represents the dependency of the liquid volume in a standard sample on the liquid volume in the test sample. This curve is obtained by separately measuring the weight of the sample at various liquid saturations and then calculating the corresponding liquid volume in each sample using the wetting liquid's density. The volume of liquid in test sample is plotted on the x-axis while the liquid volume in standard sample is plotted on the y-axis.

3. The calculated pore size distribution of test sample shown on the right side of the plot. This curve is obtained by finding x and y coordinates at point D.

As shown in Figure 4.5, the y-coordinate at point B on the second plot, which represents the volume of the liquid in a standard sample, corresponds to the y-coordinate on point C on the first plot. By assuming the wetting angles for both standard and testing sample are equal, at capillary equilibrium, the maximum radius of filled pores is equal for both

standard and testing sample. This means that the x-coordinate of point D is the same as the x-coordinate of point C. The y-coordinate of point D can also be found using the second curve. The x-coordinate at point B represents the volume of liquid in the test sample, which is the corresponding y-coordinate at point D. By using the same scale on the x-axis and y-axis on the left plot, point A is found at the intersection of the line at 45°angle and the line connecting the x-axis to point B. This point has the same x and y value, thus its y value corresponds to the y-coordinate of at point D. Hence, by measuring the liquid volume in each sample as it evaporates, the third curve is obtained through finding the coordinates of point D at different liquid volumes.

4.3.2 Sample Preparation

Samples used for the MSP are cut in shape of a disc with 23mm diameter. To increase the accuracy of measurements, 3 samples are stacked and glued together. To ensure that the pores are not filled with glue, a very small amount of glue is applied to three locations on the edges of the samples. The GDL samples along with two calibrated standard samples are left inside a vacuum chamber at a temperature of 175°C for two hours to completely dry up. After the samples are cooled down, the thickness of the GDL sample and the dry mass of all three samples are measured. The samples are then placed in octane liquid inside a vacuum chamber for half an hour to become fully saturated. Once the samples become fully saturated, they are placed in the porosimetry apparatus.

Chapter 5

Results and Analysis

In this chapter the results obtained from compression tests performed on the gas diffusion layer (GDL) are presented and analyzed. The effects of a few critical factors such as temperature, relative humidity, hydrophobic coating, and cyclic loading on the compressive behaviour of the GDL are discussed. To characterize these effects, compressive stress-strain curves along with detailed analysis of structural changes in GDL are provided. To analyze the structural changes of GDL in depth, scanning electron microscope (SEM) images of compressed and uncompressed GDLs are presented.

5.1 Compressive Stress-Strain

Although many researchers have performed compression tests on various types of GDLs, the compressive behaviour of the SpectraCarb-2050A carbon paper has not yet been studied. The compressive stress-strain curve for SpectraCarb paper obtained in this study is shown in Figure 5.1 with polynomial curve fit, and in Figure 5.2 with error bars showing the total error (bias and precision) as calculated in Chapter 4. As expected, GDL does not have a typical stress-strain behaviour. A non-linear region can be identified at low compression pressure, which indicates that the GDL is permanently deformed even at a very low compression pressure. The compressive stress-strain curve for GDL can be divided into three regions:

1. A linear region at for compression pressures of less than 0.1MPa
2. A non-linear region for compression pressures between 0.1 MPa to 1MPa

3. A linear region for compression pressures above 1MPa

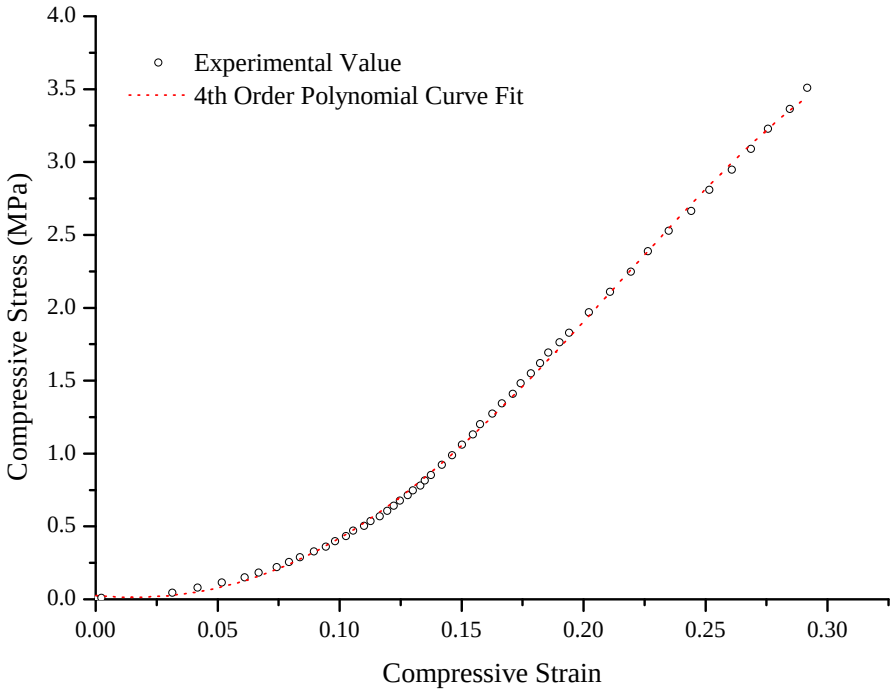

Figure 5.1: Compressive stress-strain curve for SpectraCarb 2050-A GDL obtained from experimental measurements at room temperature. A 4th order polynomial curve is fitted to the experimental values ($R^2 = 0.9993$).

In the first region of the curve, compressive strain is increased rapidly and linearly with the applied stress. The thickness of the GDL is decreased by about 5% with an applied stress of only 0.1MPa. In the second region, the compressive strain starts to increase non-linearly with the applied stress. At the end of this region, the GDL is already deformed by 15% compared to its original thickness. In the last region, the strain increases linearly again with applied stress. In this region, the GDL is less compressive and strain increases less rapidly. Similar behaviour has been reported in the literature for the GDL [58, 54, 73, 37] and a few other porous material [68, 6, 66]. In general the compressive strain of the GDL is caused by three main sources:

1. Carbon fibre slippage
2. Carbon fibre breakage
3. Actual compression of the GDL material and fibre crushing

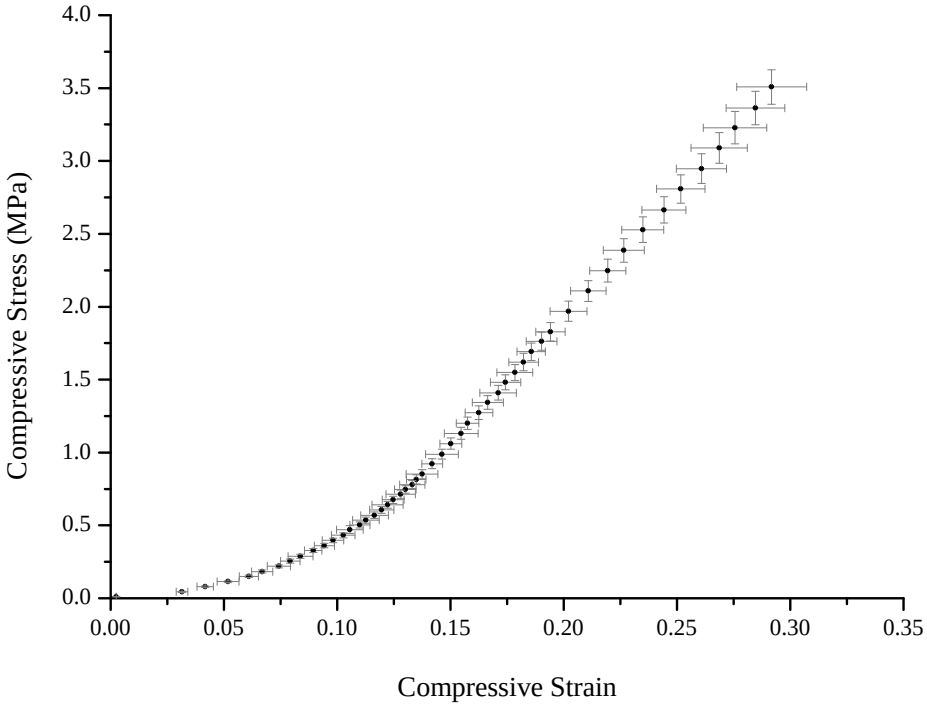

Figure 5.2: Compressive stress-strain curve for SpectraCarb 2050-A GDL at room temperature

For the range of compressive stresses considered in the present study, the change in thickness is mainly caused by carbon fibre slippage along with carbon fibre breakage. This includes all of the three regions on the compressive stress-strain curve. When the upper flux-meter comes in contact with the GDL, at first it pushes on the loose fibres at the very top of the surface of the GDL. This explains the rapid thickness reduction of the GDL in the first region. Figure 5.3 shows an SEM image taken from the cross section of an uncompressed GDL sample. As it can be seen in the SEM image, the GDL has a rough

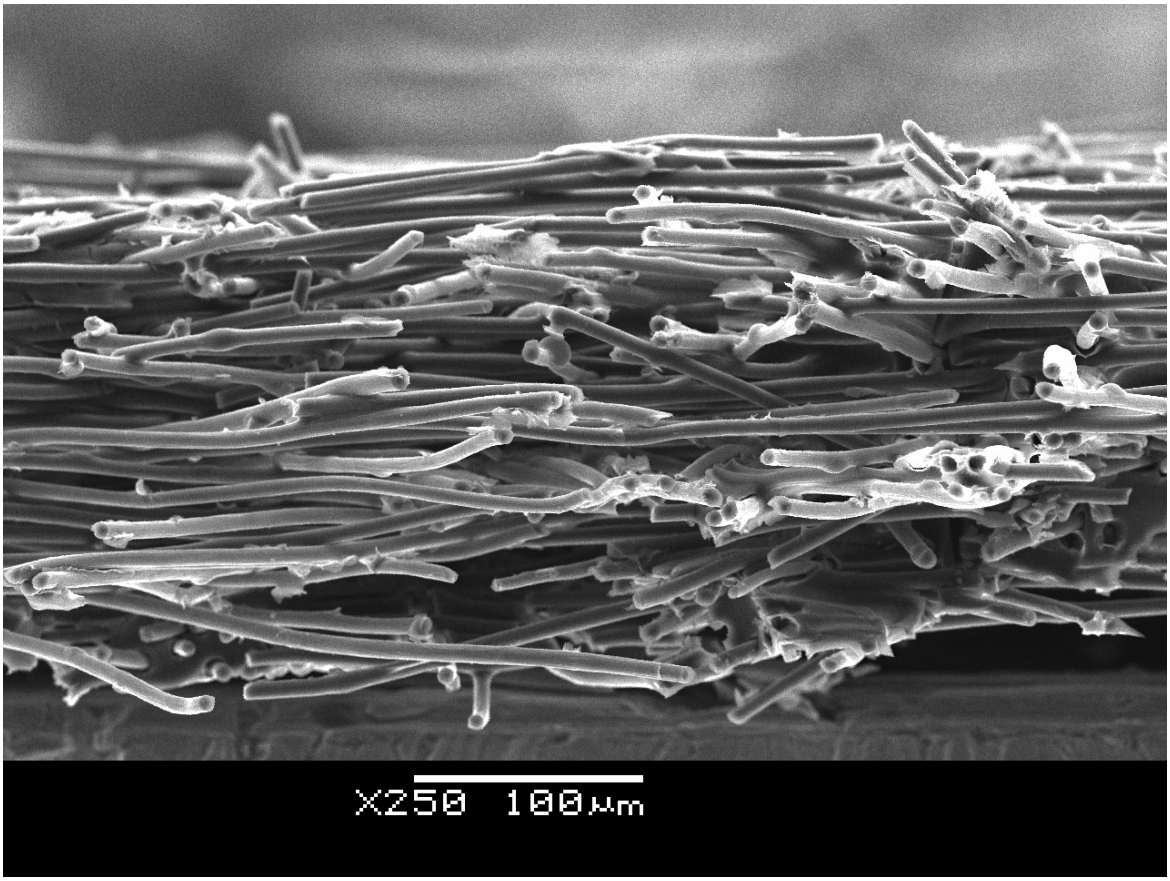

Figure 5.3: SEM image of the cross section of an uncompressed SpectraCarb-2050A GDL sample

surface and its thickness varies at different locations. Since the average thickness of the GDL is very small ($\approx 200\mu$), these thickness variations and the surface roughness are very significant ($\approx$ 15% of the average thickness).

Due to surface roughness and local thickness variation, the contact area between the GDL and the flux-meter is very small when they first come in contact. Thus, the local stress at the point of contact is much higher than the overall measured compressive stress. This is the reason why the strain increases rapidly at a low compressive stress. As the compressive stress increases and the flux-meter comes in contact with more carbon fibres, the fibres on the surface either break or slip and become dislocated, making the surface of the GDL more dense. This can clearly be seen by comparing the SEM images shown in Figure 5.5 of compressed and uncompressed GDL samples. In the SEM image of the compressed GDL

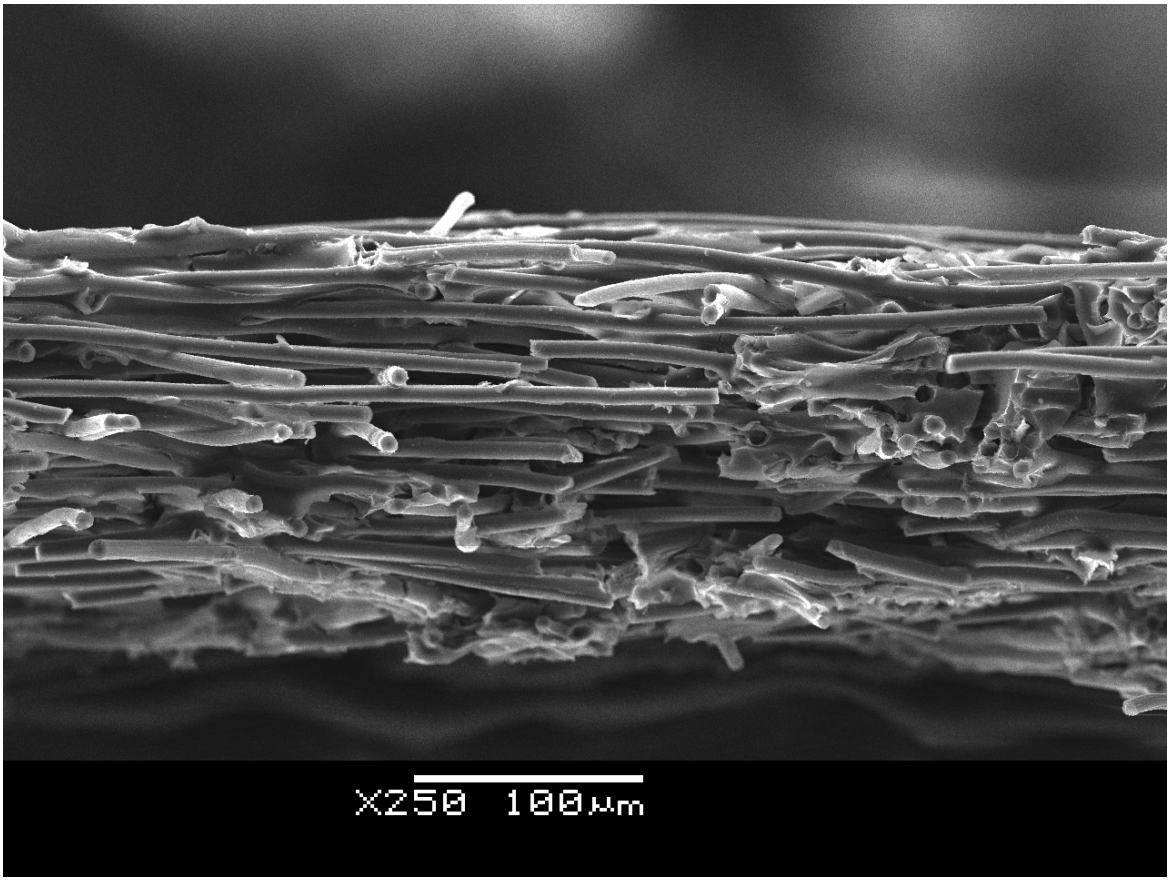

Figure 5.4: SEM image of the cross section of SpectraCarb-2050A GDL sample after being compressed by 4.7MPa

shown in Figure 5.5b, the fibres on the surface are generally closer together compared to the carbon fibres of the uncompressed GDL sample shown in Figure 5.5a. It can also be noticed that on the surface of the compressed GDL, a few of the carbon fibres are broken. As the surface becomes more dense and the contact area between the GDL and the flux-meter increases, the applied load gets distributed amongst more carbon fibres and the local stresses become smaller. This gradually decreases the rate of thickness reduction and causes the non-linearity seen in the second region.

Once the carbon fibres on the surface are fully dislocated and broken and the contact area between the GDL and flux-meter reaches its maximum, the stress transfers from the fibres on the surface to the fibres in the next layer. At this point, since the contact area between the flux-meter and the GDL does not significantly change with an increase in

compressive load, the deformation of the GDL becomes linear again, corresponding to the third region seen on the compressive stress-strain curve of the GDL. The SEM image shown in Figure 5.4, is taken from the cross section of a compressed GDL. In this figure it can clearly be seen that the local thickness of the GDL is much more uniform. The carbon fibres shown in Figure 5.4 have been dislocated and are more aligned and parallel to each other as opposed to the carbon fibres seen in Figure 5.3.

Similar results and analysis are also reported by Bazylak et al. [13]. They have taken SEM images of GDL samples after being compressed by compression pressures of 0.18 MPa, 0.36 MPa, 0.68 MPa, and 1.37 MPa. Their results indicate that the surface roughness of the GDL causes non-uniform damage on the GDL surface. However, as the pressure increases, the damage on the GDL surface becomes more isotropic. This explains the linear nature of the third region.

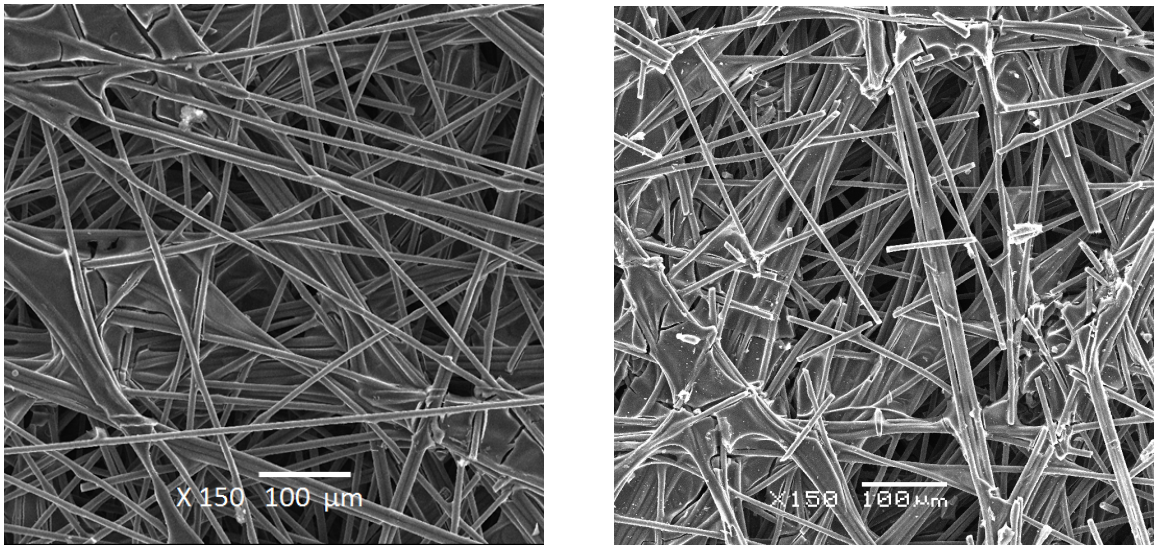

(a) Uncompressed (b) Compressed by 4.7MPa

Figure 5.5: SEM images of compressed and uncompressed SpectraCarb-2050A GDL sample taken from the top surface

For a typical compressive stress-strain curve, the compressive modulus is simply the slope of the linear region of the curve. However, as already discussed, unlike typical material, GDL does not have a linear behaviour at low compressive stress values and the rate of change in strain varies for different regions of the curve. Thus, the compressive modulus for the GDL does not have a constant value and is a function of strain itself. The compressive stress-strain curve can either be expressed as a piecewise function with 3 or

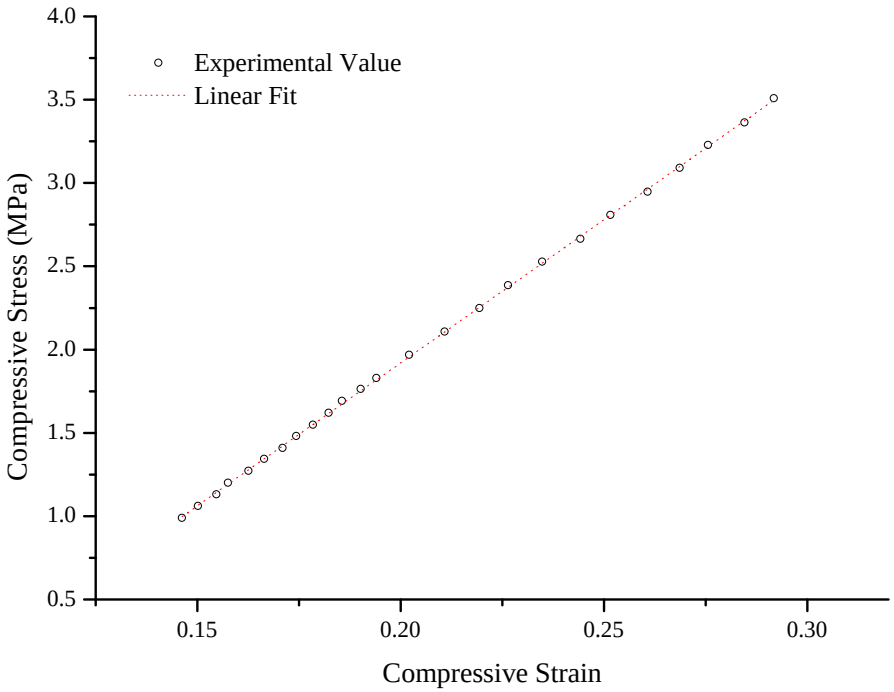

Figure 5.6: Linear curve fit for third region of GDL's stress-strain curve.

more linear regions, or as one polynomial curve. The curve fit shown in Figure 5.1 is a 4th order polynomial, which fits the data fairly well. The equation of the polynomial curve is shown in equation 5.1:

$$\sigma = -530\varepsilon^4 + 163\varepsilon^3 + 42.7\varepsilon^2 - 1.41\varepsilon + 0.0253 \tag{5.1}$$

Since the compressive modulus is simply the rate of change in stress as a function of strain, it can be estimated by finding the derivative of Equation 5.1 at any given compressive strain. The derivative of Equation 5.1 is a third order polynomial equation. Although the independent variable in the stress-strain curve is strain, it is often more practical to calculate the value of strain for a given stress and treat stress as the independent variable instead. Hence, estimation of the compressive modulus as a function of compressive strain is not very feasible. A simpler way to estimate the compressive modulus is to only consider

the rate of change in the third region. Since this region is linear, the compressive modulus will have a constant value. This is a fair assumption because in an operating fuel cell, the compressive stress is above 1MPa, which corresponds to the third region of the compressive stress-strain curve.

The third region of the compressive stress-strain curve for SpectraCarb GDL is shown in Figure 5.6. The slope of the linear fit shown in the figure has a value of 17.2, which means that the compressive modulus of SpectraCarb GDL is approximately 17.2MPa. However, since the line of best fit for the third region does not pass through the origin, to correctly estimate compressive stress at a given compressive strain or vice versa, the y-intercept of this line should also be found. The compressive strain of SpectraCarb carbon paper can then be calculated at compressive stresses above 1MPa using Equation 5.2:

$$\varepsilon = \frac{\sigma + 1.51}{17.2} \tag{5.2}$$

where ε is the compressive strain, σ is the compressive stress, 17.2 is the slope (compressive modulus), and 1.51 is the y-intercept.

5.1.1 Effect of Temperature

The operating temperature of the PEM fuel cell is typically between 65°C to 85°C. All of the current studies in literature on the GDL's compressive behaviour have only performed compression tests at room temperature. In the present study, the compressive stress-strain behaviour of the GDL is studied at various temperatures. The results obtained from this study are shown in Figure 5.7. The compressive stress-strain curves shown in Figure 5.7 are acquired from compression tests performed at 25°C, 45°C, 65°C, and 85°C. As seen in this figure, all of the four curves overlap and barely show any variation. The small variations that are seen amongst the four curves, lie within the range of measurement uncertainty and are caused by measurement error. These results suggest that for the range of temperatures that the GDL was tested for, there is no appreciable change in the compressive behaviour. Thus, the operating temperature of PEM fuel cells does not have any effect on the compressive behaviour of the GDL.

The polynomial curve fit equation, as well as the slope of the line in the linear region for each of these curves are shown in Table 5.1. Although the stress-strain curves of the GDL at different temperatures are nearly identical, the values of the constants in the polynomial curve fit equations are a bit different for each curve, while the values of the slopes of the linear portion of the curves are very close and vary by about 5% at most. Therefore, using

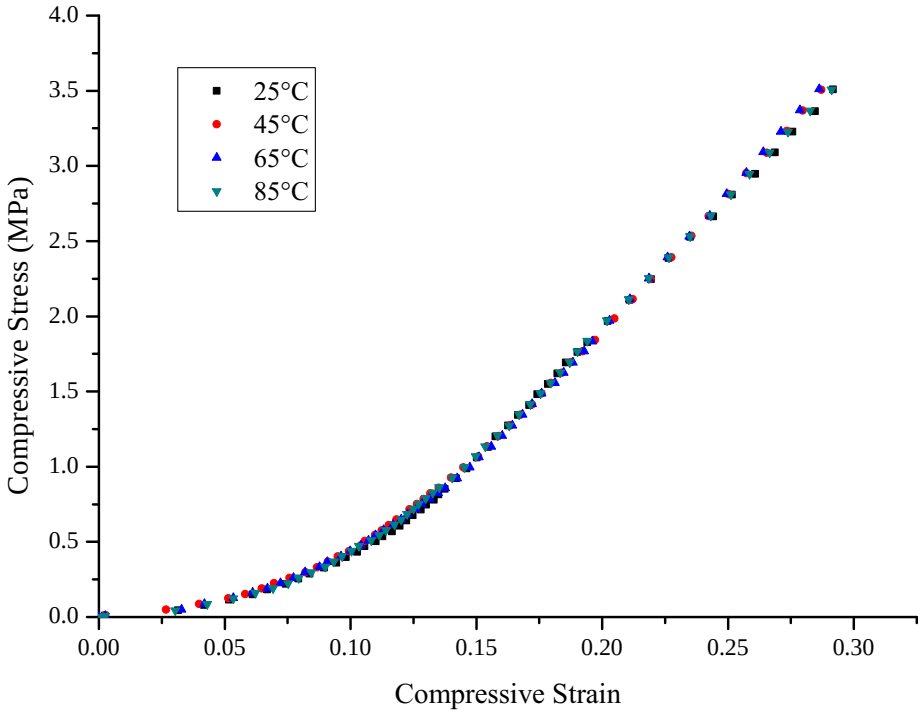

Figure 5.7: Compressive stress-strain curve for SpectraCarb-2050A GDL sample, measured at 25°C, 45°C, 65°C, and 85°C

Table 5.1: Equations of the 4th order polynomial curve fit and linear fit for the stress-strain curve of the GDL at various temperatures

Testing Temperature	Constants for Polynomial Curve Equation $\sigma = C_1\varepsilon^4 + C_2\varepsilon^3 + C_3\varepsilon^2 + C_4\varepsilon + C_5$						Linear Fit $\varepsilon = \frac{\sigma - b}{E}$		
	C_1	C_2	C_3	C_4	C_5	R^2	E	b	R^2
25°C	-530	163	42.7	-1.41	0.0253	0.9993	17.2	-1.51	0.9998
45°C	-375	120	39.7	-0.365	0.0132	0.9999	17.9	-1.65	0.9995
65°C	-525	205	26.1	0.192	0.00804	0.9998	18.2	-1.72	0.9995
85°C	-414	110	48.3	-1.29	0.0181	0.9998	17.4	-1.56	0.9998

the slope of the linear line for determining the compressive modulus of the GDL is more meaningful and better for the comparison of the obtained results.

5.1.2 Effect of Relative Humidity

In order to keep the polymer membrane fully hydrated, the PEM fuel cell operates at very high relative humidity (above 80%). High moisture content in combination with elevated temperature is generally known to reduce the strength of many composite materials. There are a significant number of studies [3, 77, 76, 4, 75, 14, 89] that focus mainly on the effect of moisture on mechanical properties of carbon-epoxy composites. All of these studies conclude that moisture causes mechanical degradation as it is absorbed by the epoxy resin matrix.

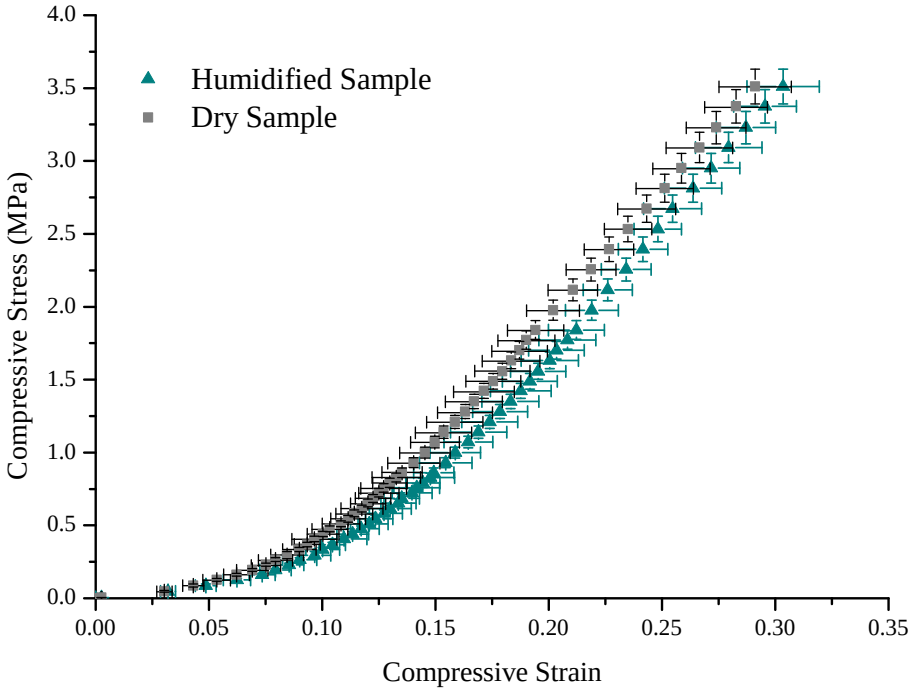

Figure 5.8: Compressive stress-strain curve for SpectraCarb-2050A GDL sample at 85°C and 0% and 85% with their estimated error bars

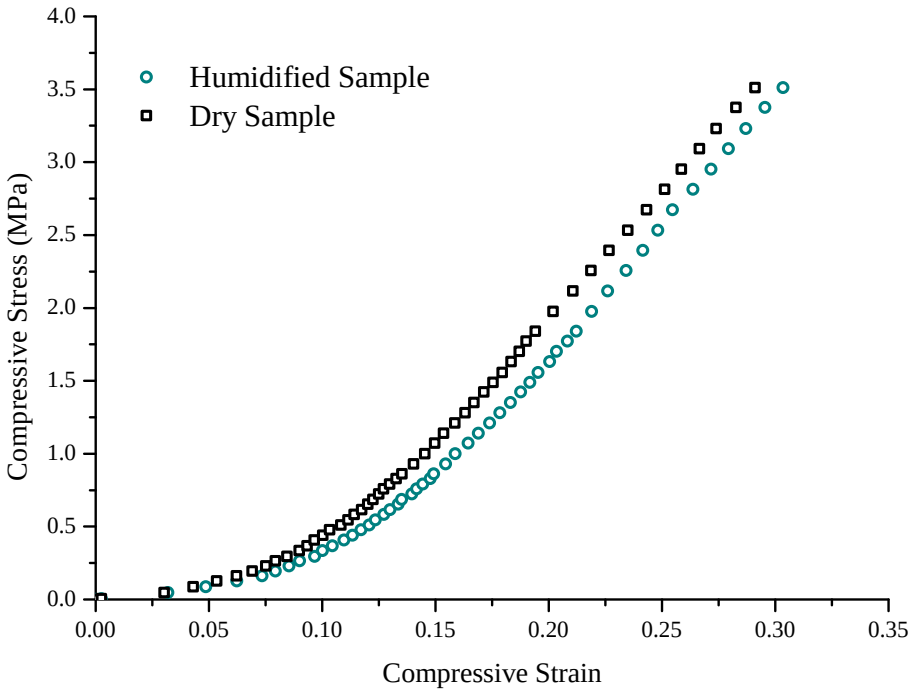

Figure 5.9: Compressive stress-strain curve for SpectraCarb-2050A GDL sample at 85°C and 0% and 85%.

The carbon paper that is used as a GDL, is also bounded by a carbonized thermoset resin and although it has a completely different structure from a carbon fibre epoxy composite, it may experience a larger deformation in a highly humid environment. The most common type of resin used in a in carbon paper GDL is phenolic resin [54]. Phenolic resin is also known to be water absorbent and may become weaker as its moisture content increases [59, 24].

To the best of the author's knowledge, no study in the literature has been conducted to measure the compressibility of the GDL in a highly humid environment. In the present study, the thickness reduction of the GDL is measured as a function of compression pressure in a highly humid environment. To clearly understand the effect of relative humidity on compressive behaviour of the GDL, compressive stress-strain curve for GDL at 85°C and 85% and 0% relative humidities are presented in Figure 5.8 (with error bars) and in

Table 5.2: Equation for the 4th order polynomial curve fit and linear fit for the stress-strain curve of the dry and humidified GDL

% RH	Constants for Polynomial Curve Equation $\sigma = C_1\varepsilon^4 + C_2\varepsilon^3 + C_3\varepsilon^2 + C_4\varepsilon + C_5$						Linear Fit $\varepsilon = \frac{\sigma - b}{E}$		
	C_1	C_2	C_3	C_4	C_5	R^2	E	b	R^2
0%	-414	110	48.3	-1.29	0.0181	0.9998	17.4	-1.56	0.9998
85%	-572.7	267	8.75	0.307	0.00641	0.9999	18	-1.96	0.9993

Figure 5.9 (without error bars).

As seen in Figure 5.9, the first region of the compressive stress-strain curve for the GDL samples at a high relative humidity is very similar to the first region on the stress-strain curve for the dry samples. As soon as the second region starts, the compressive behaviour of the humidified samples change and they become more compressible than the dry samples. This behaviour is caused by the moisture present in the carbon matrix/binder, which most likely softens the resin and makes it easier for the carbon fibres on the surface to dislocate and slip. Once the GDL samples enter the third region, their compressive strain starts to change at approximately the same rate again. There can be two possible explanations for such behaviour. One explanation, is that the moisture in the air is not successfully diffused into the pores of the GDL and only affects the outer layer (surface) of the GDL. Another explanation for the obtained results is that the effect of relative humidity becomes less significant as the structure of the GDL becomes more dense. Another factor that may contribute to the changes that are observed between the two curves, is the experimental error. However, as shown in Figure 5.8, most of the data points for both curves lie outside of the measurement uncertainty of the the other curve. This indicates that measurement error is not the only cause of the changes observed and relative humidity does actually change the compressive behaviour of the GDL.

The equations of the polynomial curve fit and linear curve fit of both of the curves are presented in table 5.2. The curve slopes, which represent the rate of change in stress as a function of strain, vary only by 3%, while their y-intercept is varied by approximately 23%. This proves that the compressibility of the GDL changes before it enters the third region.

5.1.3 Effect of Hydrophobic Coating

To prevent liquid water from flooding the pores of the gas diffusion layer, the GDL is often treated with hyrdrophobic coating. The hydrophobic coating that is used for treating the GDL is Polytetrafluoroethylene (PTFE). This treatment changes the microstructure and physical properties of the GDL. Although the effect of PTFE coating has been studied by a few researchers, in depth investigation of the the structural changes caused by the PTFE coating has not yet been conducted. The carbon paper used in this study is Toray paper (TGP-H-120), which is the most commonly used commercial GDL for PEM fuel cells.

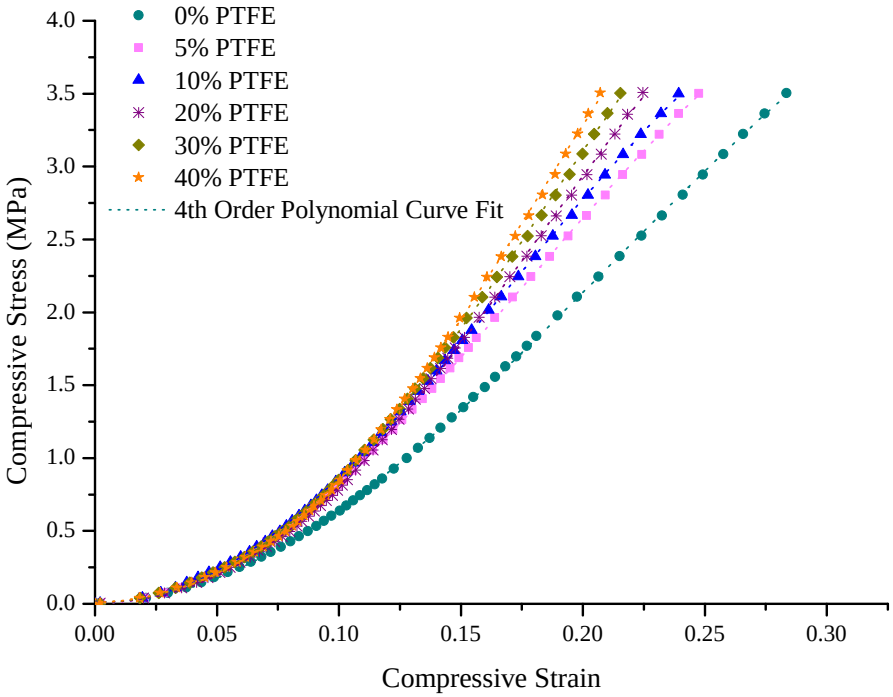

Figure 5.10: Compressive stress-strain curve for Toray paper (TGP-H-120) with 0%, 5%, 10%, 20%, 30%, and 40% PTFE treatment

The stress-strain curves obtained from compression tests performed on Toray paper with PTFE loadings of 0%, 5%, 10%, 20%, 30%, and 40% are presented in Figure 5.10. As previously mentioned, the compressive stress-strain curve for carbon paper can be

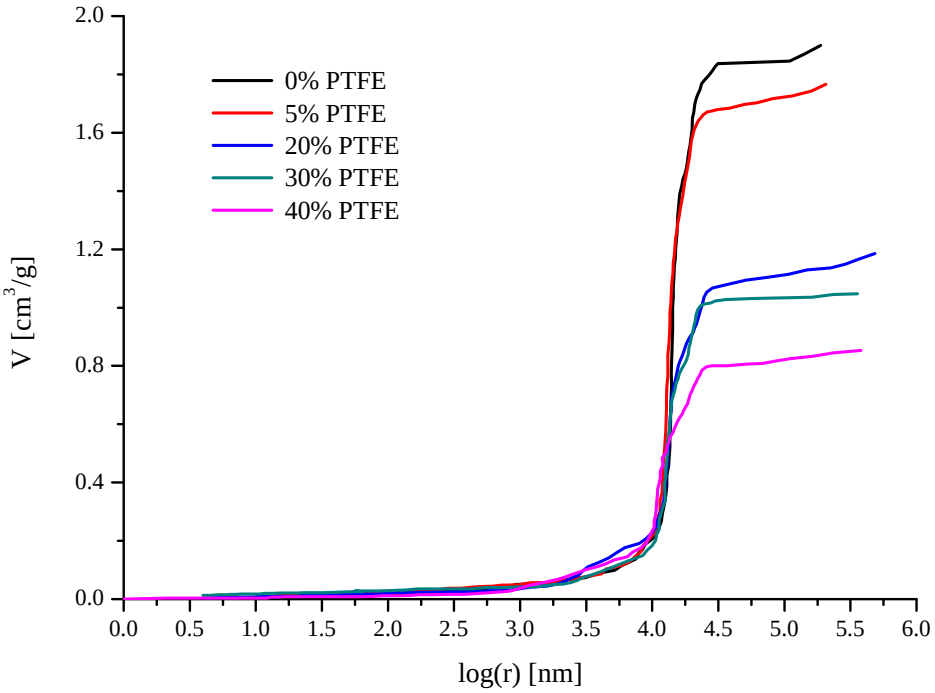

Figure 5.11: Uncompressed integral distribution of pore volume as a function of logarithmic pore radius for Toray carabon paper (TGP-H-120) with 0%, 5%, 20%, 30%, and 40% PTFE treatment

decomposed into three regions. As seen in Figure 5.10, the stress-strain curves for the treated and untreated Toray papers almost overlap in the first region. This can be explained by the surface roughness and variation in local thickness of the GDL. The first region represents the deformation of the loose carbon fibres that are located on the outer surface of the GDL and come in contact with the flux-meter first. Since the treated and untreated papers are both fabricated from the same carbon fibre material, they behave similarly within the first region. On the other hand, in the second region where the flux-meter comes in contact with the actual carbon matrix, the stress-strain curves of the untreated paper no longer overlaps with the curves for treated papers. In this region, the treated papers appear to be less compressive than the untreated paper. This is due to the fact that the PTFE treatment usually forms around the fibre connections and acts like a binding

agent and as result, improves the fibre bonding. Thus, the GDL becomes less compressive when it is treated with PTFE coating. Other studies in literature [74, 37] have also reported a decrease in compressibility for samples with PTFE coating.

As shown in Figure 5.10, the amount of PTFE loading does not actually show any appreciable effect on the compressibility of the GDL in the second region. The stress-strain curves of the carbon papers with various PTFE loadings continue to overlap in this region. This is mainly because in this region the compressibility of the GDL is still primarily influenced by the GDL's surface roughness and thickness variation and stress is not yet transferred to the inner layers of the sample. The compressive stress is then only absorbed by the surface layer of the GDL and since the inner layers are not under stress, their bulk properties such as amount of PTFE loading and porosity will not have an effect on the compressibility of the GDL at this point.

In the last region of the compressive stress-strain curve, where the inner layers of the GDL start to deform, the GDL samples with a higher PTFE loading, become less compressive. At this point, the compressibility of the GDL is influenced by its bulk properties. To better understand how PTFE coating affects the compressive behaviour of the GDL, the effect of PTFE treatment on the structural properties of the GDL such as porosity and pore size distribution is investigated using the method of direct porosimetry. Both integral and differential distributions of pore volume as a function of pore radius for uncompressed GDL samples with various PTFE loadings (0%, 5%, 20%, and 30%) are presented in Figures 5.12 and 5.11 respectively. The results presented in both of these plots, suggest that the pore volume of the gas diffusion layer decreases with an increase in PTFE content. The majority of the pore space in every tested sample consists of pores with radii of between 10μm to 20μm. Pore radius of 15μm is the most common pore radius amongst all 5 samples. As it is seen in Figure 5.12, although PTFE coating decreases the overall pore volume of the GDL, it does not actually change the maximum pore size and pore size distribution of the GDL. These results are in good agreement with the results obtained by other studies in the literature [52].

With the information obtained from the pore volume distribution curves, the compressive behaviour of the treated GDL samples can easily be explained in the the third region. As the PTFE content increases, the compressibility and total pore volume of the GDL decrease. This shows a direct relation between porosity and compressibility of the GDL. Less pore volume makes it harder for the carbon fibres to move and dislocate. As the pressure increases and the pore volume decreases, the GDL becomes less and less compressible. The effect of volume reduction is more significant for samples with higher PTFE loading. This is because as the total volume decreases, the ratio of pore volume occupied by PTFE becomes larger and its effect becomes more significant. This explains why the slope of the

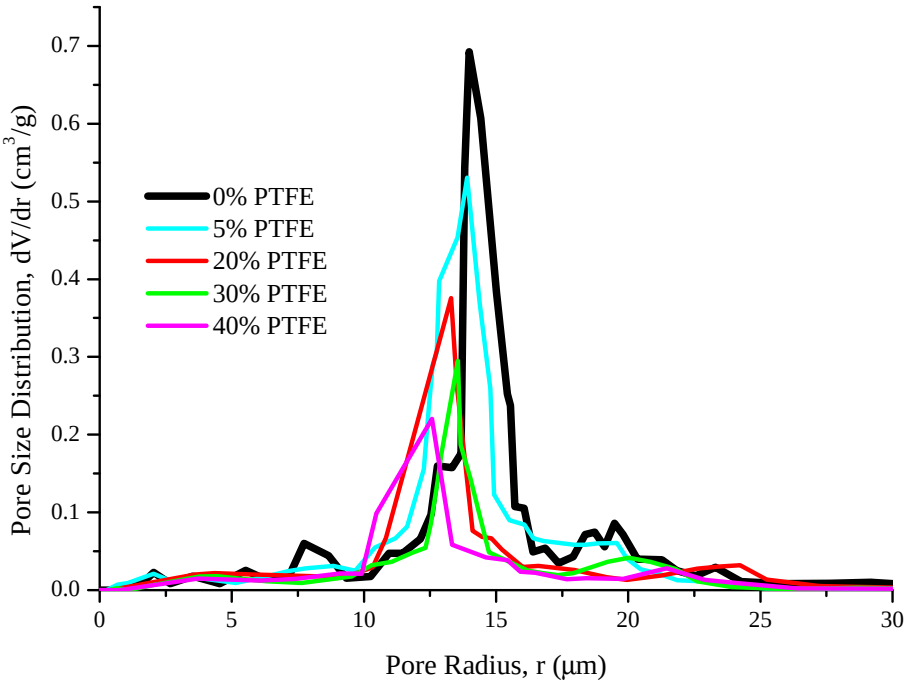

Figure 5.12: Uncompressed differential distribution of pore volume as a function of pore radius for Toray carbon paper GDL (TGP-H-120) with 0%, 5%, 20%, 30%, and 40% PTFE treatment

line in the third region of stress-strain curve for GDL samples with higher PTFE loading becomes steeper.

Another interesting behaviour that can be observed from Figure 5.10 is that the third regions of all of these curves starts at an approximately same compressive strain, which means that the three regions on the compressive stress-strain curve are controlled by the compressive strain as opposed to compressive stress. This proves that the compressive behaviour of the GDL in the second region is primarily caused by the surface roughness and thickness variations, which is approximately equal for all of the tested samples.

The equations of the polynomial curve fits and linear curve fits for all tested GDL samples are summarized in Table 5.3. As shown in this table, the slopes obtained from the third region become larger with an increase in PTFE loading. Since the third region

Table 5.3: Equation of 4th order polynomial curve fit and slope of the linear fit for the stress-strain curve of Toray carbon paper (TGP-H-120) GDL with various PTFE content

PTFE Coating	Constants for Polynomial Curve Equation $\sigma = C_1\varepsilon^4 + C_2\varepsilon^3 + C_3\varepsilon^2 + C_4\varepsilon + C_5$						Linear Fit $\varepsilon = \frac{\sigma - b}{E}$		
	C_1	C_2	C_3	C_4	C_5	R^2	E	b	R^2
0%	-31.6	107	77.0	0.244	0.0110	0.9999	16.2	-1.10	0.9999
5%	-8.56	-207	112	-0.986	0.0115	0.9998	18.6	-1.08	0.9999
10%	-136	-180	116	-1.18	0.0609	0.9998	19.2	-1.09	0.9999
20%	-772	134	80.6	-0.700	0.0148	0.9998	22.2	-1.52	0.9994
30%	-808	157	79.3	-0.207	0.0122	0.9998	23.4	-1.60	0.9989
40%	-1600	-505	40.4	0.933	0.00743	0.9998	25.5	-1.84	0.9985

for the samples with PTFE treatment starts at a higher compressive stress, the linear fit provided in the table can only be used for compressive stresses above 1.3MPa.

5.1.4 Comparison to Existing Literature

As mentioned earlier, compressive behaviour of the SpectraCarb paper is measured for the first time in the present study. Hence, there are no current studies in the literature that can be used for comparing these results. Unlike SpectraCarb paper, the compressive behaviour of Toray paper has been studied by a few researchers. The compressive behaviour of Toray paper with 10% PTFE obtained by Esribano et al. [25] is shown in figure Figure 5.13. The results obtained from the present study agrees well with the results obtained by Escribano et al.

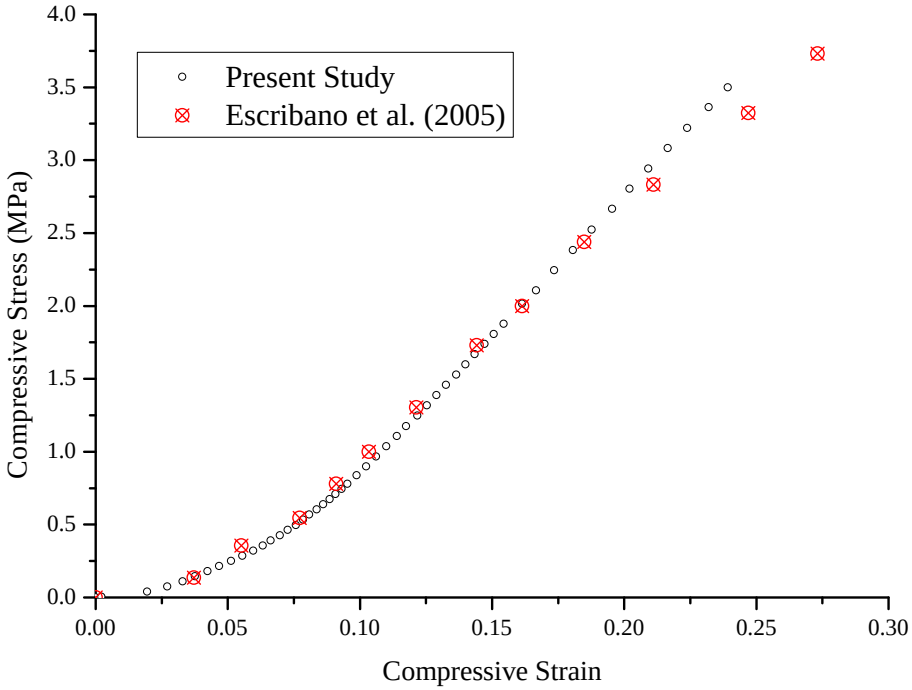

Figure 5.13: Compressive stress-strain curve for Toray paper with 10% PTFE obtained from the present study and study by Escribano et al. [25]

5.2 Cyclic Compression

In an operating PEM fuel cell, the gas diffusion layer (GDL) is constantly under a compressive load that is caused by the clamping force. The fuel cell's operating conditions (temperature$\approx 85°C$ and relative humidity$\approx$90%) in a combination with the ongoing chemical reactions lead to a non-uniform hygro-thermal loading inside the fuel cell. These non-uniform hygro-thermal loadings lead to a non-uniform stress distribution on the GDL. Because the magnitude of these stresses constantly vary, they are considered to have a cyclic nature. Cyclic loading is simply continuous loading and unloading of a material for a number of cycles.

5.2.1 Effect of Cyclic Compression on GDL Thickness

As previously discussed in Chapter 3, there are only a few studies in the literature that investigate the effects of loading and unloading cycles on the structure and mechanical properties of the GDL. The maximum number of cycles the GDL has been so far tested for is 10 cycles. In an actual fuel cell where the GDL is constantly under non-uniform and unsteady compression, performing cyclic compression test for only 10 cycles would not be sufficient to simulate the effect of hygro-thermal stresses. On a different note, hygro-thermal stresses are not the only type of cyclic compression that GDL experiences. Since the hygro-thermal stresses dissipate when the fuel cell is shut down, and become present again when the fuel cell starts, the simple act of shutting down and starting up of the fuel cell has a cyclic effect on the GDL. The durability target for a fuel cell to be used in a car is estimated to be at least 30,000 shut-down/start up cycles, which means the GDL material should be able to withstand at least 30,000 cycles of loading and unloading.

To the best of the author's knowledge, currently there are not any studies in the literature that investigate the effect of loading and unloading on the GDL over a reasonably large number of cycles. In this study the change in thickness of the GDL is measured for over 2500 cycles for the first time. To simulate the start-up/shut-down effect of the PEM fuel cell on the GDL, SpectraCarb-2050A is first compressed by a compression pressure of 2MPa and then is compressed by reduced pressure of 1MPa and then the pressure is back to 2MPa and this cycle repeats for a number of 2500 cycles. Due to time limitations, this experiment is only repeated once. In Figure 5.14, the compressive strain measured at 2MPa is plotted as a function of cycle number for two stacks of GDL samples.

As depicted in Figure 5.14, the compressive strain of both sets of tested samples continuously increases for up to 1500 cycles. A couple of sudden jumps can be spotted on both of the curves. The first jump for both of these curves is seen at early cycles and is caused by the original deformation of the GDL. When the GDL is compressed for the first time, the material will become damaged and will deform easier the second time it becomes compressed. Other studies in the literature [54, 25, 53, 72] have also reported a noticeable increase in strain after the first cycle. After a few cycles of compression, the carbon fibres be dislocate and move closer together and become more resistant to a compressive load. The remaining sudden jumps can be explained similarly. To reduce measurement uncertainty, 6 samples are stacked together for each cyclic compression test. As discussed earlier, the applied stress is not distributed evenly through every layer of the GDL. During the early cycles of the test, most of the applied pressure is absorbed by the top and bottom layers that are directly in contact with the flux-meters. Repeated cycles of compression eventually crushes the top and bottom layers and the stress will then get passed on to the

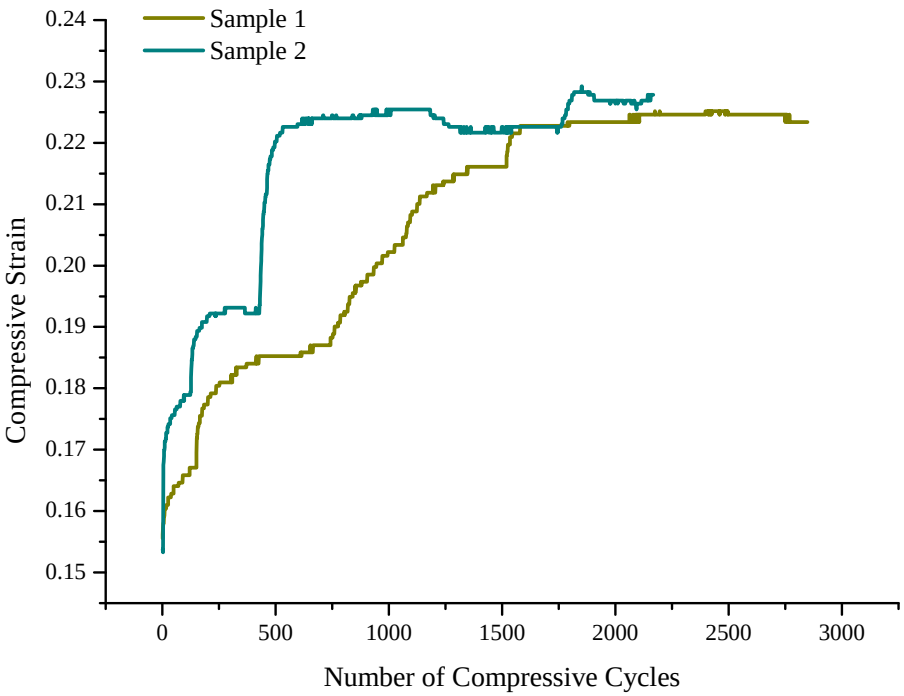

Figure 5.14: Change in compressive strain in SpectraCarb 2050A as a function of cycle number for loading cycles of 2MPa and unloading cycles of 1MPa.

neighbouring samples. Thus, jumps on the curve that occur at later cycles, correspond to the point where the samples on the surface are completely crushed and the stress is transferred to the next layer of samples.

Although the rate of change in strain for the two stacks of samples are slightly different, they both reach a constant value after approximately 2000 compressive cycles. The difference in the shape of the curves for the two samples can be explained by the random structure of the GDL and measurement errors. The final strain measurements after 2500 cycles indicate a 50% increase in strain compared to the initial state of the experiment. It should be noted that since this experiment has only been performed on two sets of samples, the uncertainty and repeatability of the results are unknown. For more meaningful conclusions to be drawn, this experiment should be repeated a few more times.

5.2.2 Effect of Loading/Unloading on The Structure of GDL

To get a better understanding of the changes in microstructure of the GDL during loading and unloading cycles, the thickness of a stack of GDL samples are measured during 7 loading and unloading cycles. The stress-strain curve obtained from the first loading/unloading cycle is presented in Figure 5.15. The stress-strain curve corresponding to the unloading, shows irreversible damage caused by the deformation of the GDL during loading. Although the pressure on the sample is released the same way that it was applied, the unloading curve does not follow the same path as the loading curve.

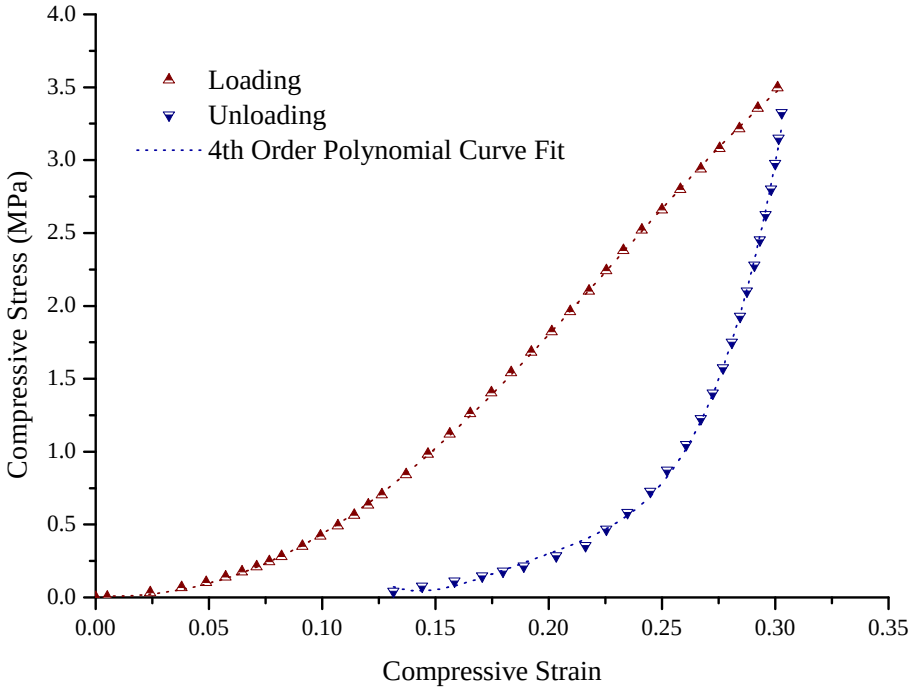

Figure 5.15: Stress-strain curve obtained from the first loading/unloading cycle of the GDL

The unloading curve starts with a very steep slope which indicates that the strain decreases very slowly as the stress decreases. After about 5% of the strain is recovered, the rate of change in strain increases rapidly and non-linearly. The strain starts to decrease linearly again once more than 10% of the strain is recovered. At this point the strain

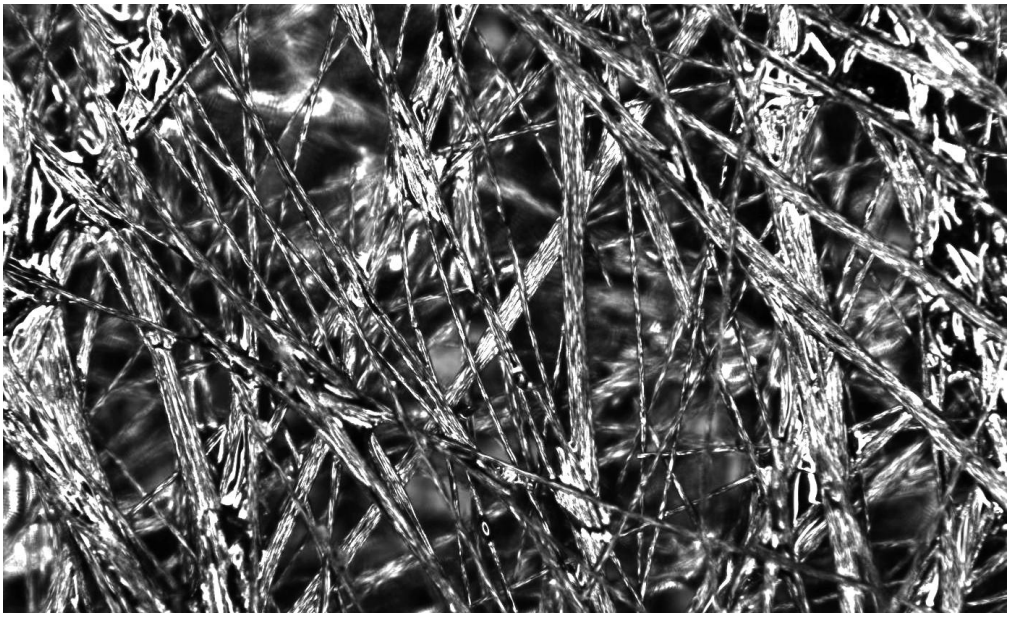

Figure 5.16: Electron microscopy image of uncompressed GDL taken at 172.0X magnification and 90% Aperture

decreases very rapidly. The rate at which the strain decreases in this region is comparable to the rate of increase in strain at the first region of the loading curve.

During the initial stage of unloading, the strain does not recover quickly because the GDL has already become plastically deformed. The carbon fibres that are broken or debonded and dislocated do not resume their original shape and position. These fibres become tangled and get stuck between other fibres and mostly remain at the same location while the GDL is being unloaded. As the flux-meter reduces the pressure and moves upwards, less carbon fibres are in contact with it. With reduction in contact area between the flux-meter and GDL surface, the actual applied stress on the GDL's surface is higher than the measured value. Similar to the second region of the loading curve, this region of the unloading curve is non-linear due to changes in the contact are between the flux-meter and the GDL. Once the contact area between the GDL and flux-meter becomes uniform, the strain starts to decrease rapidly. This is due to the fact that the GDL material is weaker after the initial loading cycle.

The electron microscopy images shown in Figures 5.16 and 5.17 are taken from the GDL sample before and after the first loading/unloading cycle. As seen in these figures, the GDL is more dense after the first cycle. Although the carbon fibres shown in Figure 5.17 do not

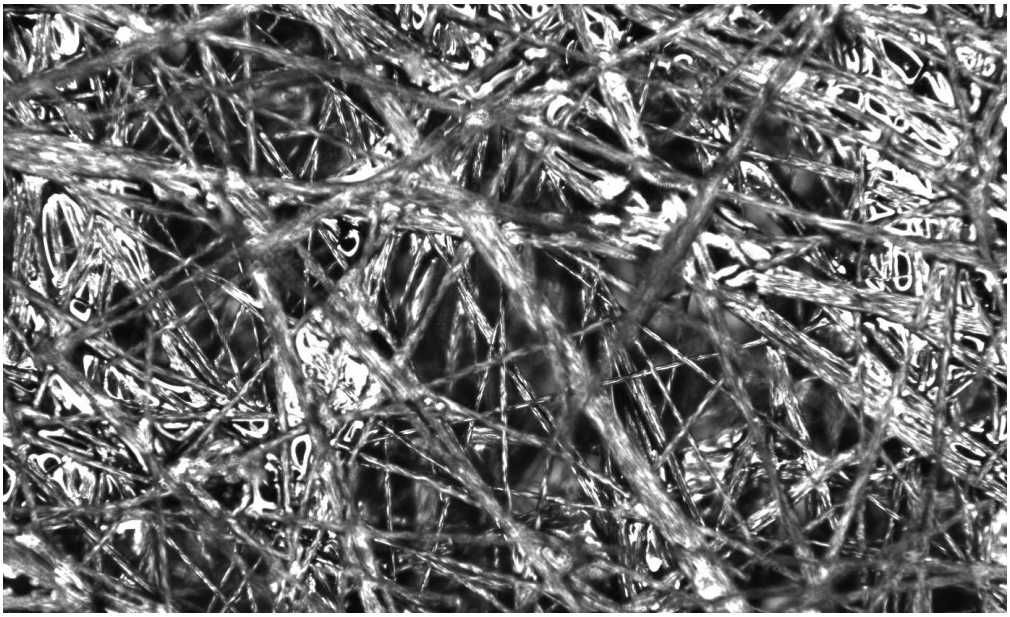

Figure 5.17: Electron microscopy image of GDL taken after 1 compressive cycle at 172.0X magnification and 90% Aperture

look damaged or broken, the structure of the GDL is plastically deformed by dislocation of the fibres.

Figure 5.18 shows the stress-strain behaviour of the GDL sample throughout 7 loading and unloading cycles. The compressive behaviour of the GDL during the second cycle is very different than the first cycle. The first region of GDL's compressive stress-strain curve is very small during the initial loading cycle. After the first cycle, this region is expanded to a higher range of compressive stresses. On the other had, the third region of the repeated loading curves is smaller. As shown previously, the surface of the GDL becomes more uniform after the first compression. This is why a larger linear region is obtained in the second cycle.

After the first cycle, the shape of the loading curves starts to look similar to the shape of the unloading curves and as the number of cycles increases, their shape becomes more similar. This is due to the irreversible damages that are caused after each cycle. These irreversible damages can clearly be seen in the electron microscopy image shown in Figure 5.19, which is taken from the sample after the seventh cycle. The electron microscopy image of the GDL indicates formation of cracks on the surface of the GDL. The original structure and orientation of carbon fibres are completely changed and the

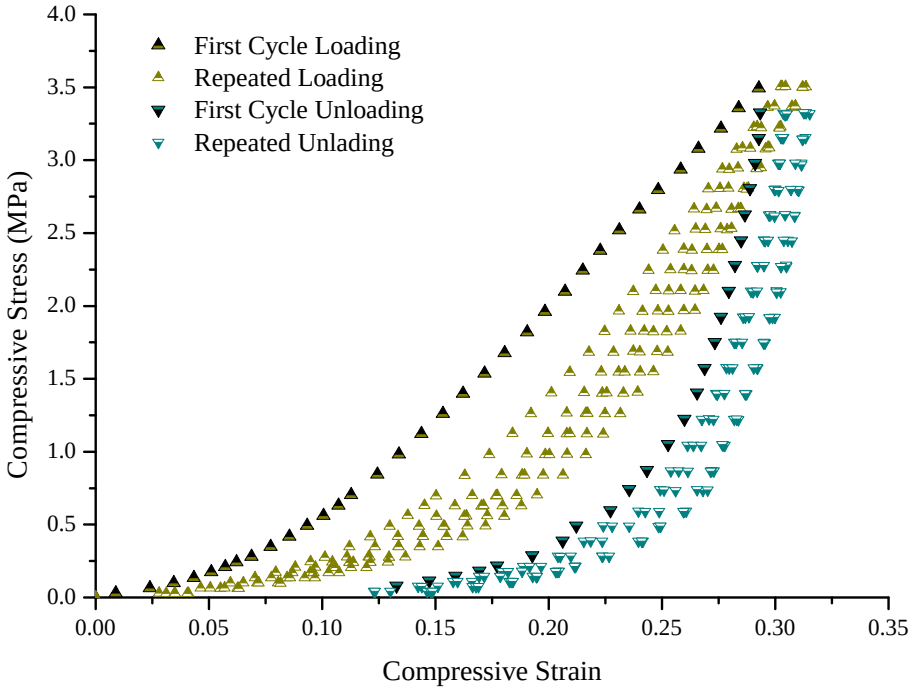

Figure 5.18: Compressive stress-strain curve of the GDL corresponding to seven loading/unloading cycles

fibres are crushed into smaller pieces. Broken pieces of the carbon fibres are tangled and packed closer together.

The change in initial thickness of the GDL after each cycle is measured. The corresponding residual strain is plotted against the number of cycles and is represented in Figure 5.20. The residual strain increases after each cycle, which means that after every cycle the uncompressed thickness of the GDL becomes smaller. The original thickness of the sample is decreased by 14% after 7 cycles. This thickness reduction is caused by carbon fibre breakage and dislocation towards the inner layer of the GDL.

The thickness reduction of the GDL reduces the porosity and blocks the path of the reactants to the catalyst layer. The deformation and change in microstructure of the GDL after seven loading and unloading cycles are very significant. This degree of deformation can severely degrade the performance and durability of PEM fuel cells. Although the actual

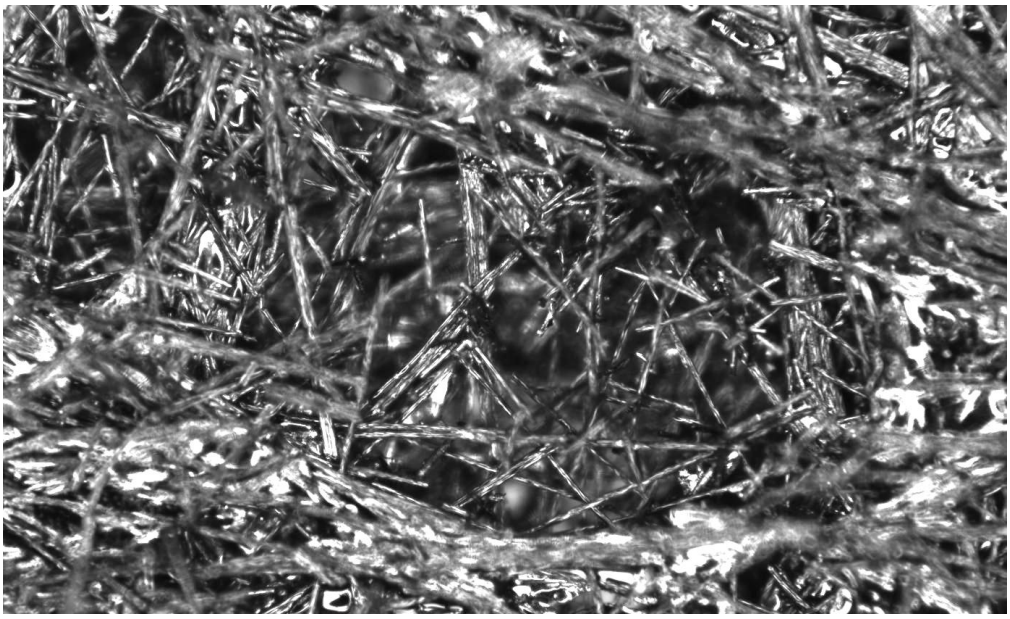

Figure 5.19: Electron microscopy image of GDL taken after 7 compressive cycles at 172.0X magnification and 90% Aperture

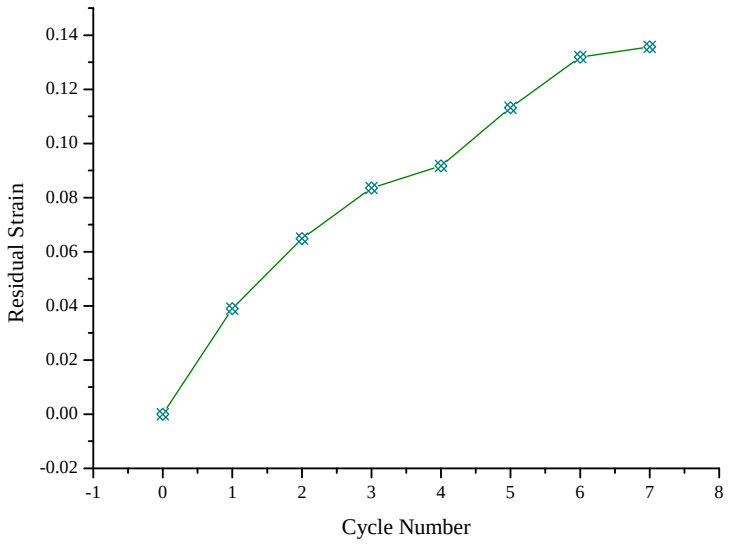

Figure 5.20: Change in original thickness of the GDL after each cycle

operating pressure of the PEM fuel cell is much lower than the maximum compression pressure tested in this study, it can still be concluded that the GDL performs very poorly under cyclic loading and durability is one of GDL's major drawbacks.

Chapter 6

Conclusions and Recommendations

6.1 Conclusions

The durability of a polymer electrolyte membrane (PEM) fuel cell is strongly dependant on the performance of the gas diffusion layer (GDL). The GDL in an assembled fuel cell is always under compression by the clamping force. Since the GDL is highly porous, its physical properties are strongly dependant on its compressibility.

In the present study, the compressive behaviour of the GDL is investigated by performing numerous compression tests. The thickness of the GDL is measured as a function of applied compressive load. The obtained results are analyzed in the form of compressive stress-strain curves. The compressive stress-strain curve of the GDL can be divided into three distinct regions: a small linear region at very low compression pressures, a non-linear region for compression pressures below 1MPa, and a linear region for the compression pressures greater than 1MPa, at which the strain increases less rapidly. It is concluded that the first two regions of the stress-strain curve are induced by surface roughness and thickness variation along the surface of the GDL sample. Since the rate of change of the strain is not constant in GDL's compressive stress-strain curve, the compressive modulus of the GDL is a function of strain itself. The compressive modulus of GDL is estimated and presented using two methods. In the first method, an appropriate 4th order polynomial curve is found to fit all three regions of GDL's stress-strain curve. The second way is to calculate the slope and y-intercept of the line that fits the third region of GDL's stress-strain curve. The second method is concluded to be more meaningful for the analysis of the results.

The effects of PEM fuel cell's operating conditions, such as temperature and relative humidity, and hydrophobic treatment of the GDL, are investigated on the compressive

behaviour of the GDL. Compressive stress-strain curves are obtained for GDLs at 25°C, 45°C, 65°C and 85°C. It is concluded that temperature has no appreciable effect on the compressibility of the GDL within the experimental margin of error. The compressive stress-strain curve obtained for GDL samples at 85°C with 85% relative humidity suggest that high relative humidity changes the compressive behaviour of the GDL in the second region of the compressive stress-strain curve and increases the compressibility. The effect of PTFE coating on compressive behaviour of the GDL is studied by performing compression tests and measuring the pore size distribution of uncompressed GDL samples with various PTFE content. It is concluded that PTFE coating decreases the total pore volume of the GDL, which consequently decreases GDL's compressibility. The amount of PTFE coating only affects the third region of the compressive stress-strain curve. Samples with higher PTFE content have lower porosity and are less compressive.

To investigate the effects of cyclic loading, the changes in thickness of two sets of GDL samples are measured at loading and unloading cycles of 2MPa and 1MPa respectively for a total number of 2500 cycles. Both sets of the GDL samples show a 50% increase in strain after 2500 compression cycles. The thickness of the GDL samples eventually reaches a constant value after 1500 cycles. To further investigate the effect of unloading on the compressive behaviour of the GDL, stress-strain curves for 7 cycles of loading and unloading are measured. It is concluded that the GDL permanently deforms and becomes weaker each time it is loaded and unloaded with a compressive force. The electron microscopic images of the GDL show that the carbon fibres break into smaller pieces and form cracks on the surface of the GDL. The microstructural changes of GDL become very significant after only a few compression cycles, which concludes that durability of the GDL tremendously decreases under cyclic compression.

6.2 Recommendations

In order to further expand this work, future research in this field should include:

- Investigation of the effect of cyclic loading at a compression pressure close to a PEM fuel cell's operating pressure. This includes performing cyclic loading and unloading tests on GDL samples as well as studying the microstructural changes by taking SEM images of the sample before and after the compression cycles
- Investigation of the effect of stacking samples. This includes performing compression tests on stacks of GDLs with different number of samples, as well as studying the

microstructural changes by taking SEM images of the samples at different layers of the stack after they become compressed.

- Further investigation of the effect of relative humidity by performing compression tests at various levels of relative humidity and temperature.
- Investigation of the combined effect of cyclic compression and relative humidity
- Investigation of the difference between pore size distribution of compressed and uncompressed GDL samples
- Investigation of the compressive behaviour of the entire membrane electrode assembly (MEA). It is recommended to perform compression tests at high relative humidity conditions to further investigate the effect of membrane swelling on the compressive behaviour of the MEA.

In order to improve the experimental method for future studies, a few recommendations regarding the testing apparatus are proposed:

- Using the same heat source for both top and bottom flux-meters to ensure uniform temperature along the sample.
- Using a non-corrosive material for the flux-meters so that they would not become damaged while testing at high relative humidities
- Using a material with extremely low thermal expansion for the flux-meters. Since the thickness of the test samples is very small, even small amount of thermal expansion can have a significant effect the accuracy of thickness measurements.
- Using a load cell that can measure larger loads so that larger test samples can be used. This would decrease the measurement uncertainty associated with the area and misalignment of the stacked samples.

References

[1] The method of standard porosimetry: 1. principles and possibilities. *Journal of Power Sources*.

[2] Contact resistance prediction and structure optimization of bipolar plates. *Journal of Power Sources*, 159(2):1115 – 1122, 2006.

[3] Donald F Adams and A Keith Miller. Hygrothermal microstresses in a unidirectional composite exhibiting inelastic material behavior. *Journal of Composite Materials*, 11(3):285–299, 1977.

[4] R.D. Adams and M.M. Singh. The dynamic properties of fibre-reinforced polymers exposed to hot, wet conditions. *Composites Science and Technology*, 56(8):977 – 997, 1996.

[5] Johan Andr, Laurent Antoni, Jean-Pierre Petit, Eric De Vito, and Alexandre Montani. Electrical contact resistance between stainless steel bipolar plate and carbon felt in pefc: A comprehensive study. *International Journal of Hydrogen Energy*, 34(7):3125 – 3133, 2009.

[6] M.F. Ashby and R.F.Mehl Medalist. The mechanical properties of cellular solids. *Metallurgical Transactions A*, 14(9):1755–1769, 1983.

[7] Bharat Avasarala, Richard Moore, and Pradeep Haldar. Surface oxidation of carbon supports due to potential cycling under {PEM} fuel cell conditions. *Electrochimica Acta*, 55(16):4765 – 4771, 2010.

[8] M. Bahrami, M. M. Yovanovich, and J. R. Culham. A compact model for spherical rough contacts. *Journal of Tribology*, 127(4):884, 2005.

[9] R. K. Bansal. *A Textbook of Strength of Materials*. Laxmi Publications, 5 edition, 2012.

[10] Frano Barbir. Chapter 4 - 4. main cell components, materials properties and processes. In {*PEM*} *Fuel Cells*, pages 73 – 113. Academic Press, Burlington, 2005.

[11] Frano Barbir. Pem fuel cells. In *Fuel Cell Technology*, Engineering Materials and Processes, pages 27–51. Springer London, 2006.

[12] Frano Barbir. Chapter one - introduction. In {*PEM*} *Fuel Cells*, pages 1 – 16. Academic Press, Boston, second edition edition, 2013.

[13] A. Bazylak, D. Sinton, Z.-S. Liu, and N. Djilali. Effect of compression on liquid water transport and microstructure of {PEMFC} gas diffusion layers. *Journal of Power Sources*, 163(2):784 – 792, 2007.

[14] E.C. Botelho, L.C. Pardini, and M.C. Rezende. Hygrothermal effects on the shear properties of carbon fiber/epoxy composites. *Journal of Materials Science*, 41(21):7111–7118, 2006.

[15] Odne S. Burheim, Jon G. Pharoah, Hannah Lampert, Preben J. S. Vie, and Signe Kjelstrup. Through-plane thermal conductivity of {PEMFC} porous transport layers. *Journal of Fuel Cell Science and Technology*, 8(2):021013, 2011.

[16] O.S. Burheim, G. Ellila, J.D. Fairweather, A. Labouriau, S. Kjelstrup, and J.G. Pharoah. Ageing and thermal conductivity of porous transport layers used for {PEM} fuel cells. *Journal of Power Sources*, 221(0):356 – 365, 2013.

[17] Statistics Canada. Human activity and the environment: Annual statistics. 1(16-201-XIE):9–10, 2006.

[18] W.R. Chang, J.J. Hwang, F.B. Weng, and S.H. Chan. Effect of clamping pressure on the performance of a {PEM} fuel cell. *Journal of Power Sources*, 166(1):149 – 154, 2007.

[19] P.H. Chi, S.H. Chan, F.B. Weng, Ay Su, P.C. Sui, and N. Djilali. On the effects of non-uniform property distribution due to compression in the gas diffusion layer of a {PEMFC}. *International Journal of Hydrogen Energy*, 35(7):2936 – 2948, 2010.

[20] Deborah Chung. *Carbon fiber composites*. Butterworth-Heinemann, 1994.

[21] J.R. Culham, P. Teertstra, I. Savija, and M.M. Yovanovich. Design, assembly and commissioning of a test apparatus for characterizing thermal interface materials. In *Thermal and Thermomechanical Phenomena in Electronic Systems, 2002. ITHERM 2002. The Eighth Intersociety Conference on*, pages 128–135, 2002.

[22] N. de las Heras, E. P. L. Roberts, R. Langton, and D. R. Hodgson. A review of metal separator plate materials suitable for automotive {PEM} fuel cells. *Energy Environ. Sci.*, 2(2):206, 2009.

[23] F. A. L. Dullien. Structure of porous media. In *Transport Processes in Porous Media*, pages 3–41. Springer Netherlands, 1991.

[24] N.B.C. Engineers. *Phenolic Resins Technology Handbook*. NIIR Project Consultancy Services, 2007.

[25] Sylvie Escribano, Jean-Franois Blachot, Jrmy Ethve, Arnaud Morin, and Renaut Mosdale. Characterization of {PEMFCs} gas diffusion layers properties. *Journal of Power Sources*, 156(1):8 – 13, 2006.

[26] N.A. Fleck. Compressive failure of fiber composites. volume 33 of *Advances in Applied Mechanics*, pages 43 – 117. Elsevier, 1997.

[27] Pablo A. Garca-Salaberri, Marcos Vera, and Ramn Zaera. Nonlinear orthotropic model of the inhomogeneous assembly compression of {PEM} fuel cell gas diffusion layers. *International Journal of Hydrogen Energy*, 36(18):11856 – 11870, 2011.

[28] H.A. Gasteiger, J.E. Panels, and S.G. Yan. Dependence of {PEM} fuel cell performance on catalyst loading. *Journal of Power Sources*, 127(12):162 – 171, 2004. Eighth Ulmer Electrochemische Tage.

[29] Jiabin Ge, Andrew Higier, and Hongtan Liu. Effect of gas diffusion layer compression on {PEM} fuel cell performance. *Journal of Power Sources*, 159(2):922 – 927, 2006.

[30] Herbert Giesche. Mercury porosimetry: A general (practical) overview. *Particle & Particle Systems Characterization*, 23(1):9–19, 2006.

[31] H Thomas Hahn and Jerry G Williams. Compression failure mechanisms in unidirectional composites. In *Composite materials: Testing and design (seventh conference), ASTM STP*, volume 893, pages 115–139, 1986.

[32] R. C. Hibbeler. *Mechanics of Deformable Materials*. Pearson Practice Hall, 3 edition, 2008.

[33] Nancy Hofmann. Canadas growing population and its environmental influence, 1956 to 2006. *EnviroStats*, 1(16-002-XIE):10, 2007.

[34] Jari Ihonen, Frdric Jaouen, Gran Lindbergh, and Gran Sundholm. A novel polymer electrolyte fuel cell for laboratory investigations and in-situ contact resistance measurements. *Electrochimica Acta*, 46(19):2899 – 2911, 2001.

[35] Aspen Aerogels Inc. Pyrogel xt data sheet, 2012.

[36] Greenlight Innovation. Porosimeter equipment - pore size distribution measurement, 2014.

[37] M. S. Ismail, A. Hassanpour, D. B. Ingham, L. Ma, and M. Pourkashanian. On the compressibility of gas diffusion layers in proton exchange membrane fuel cells. *Fuel Cells*, 12(3):391–397, 2012.

[38] M.S. Ismail, T. Damjanovic, D.B. Ingham, M. Pourkashanian, and A. Westwood. Effect of polytetrafluoroethylene-treatment and microporous layer-coating on the electrical conductivity of gas diffusion layers used in proton exchange membrane fuel cells. *Journal of Power Sources*, 195(9):2700 – 2708, 2010.

[39] G. Karimi, X. Li, and P. Teertstra. Measurement of through-plane effective thermal conductivity and contact resistance in {PEM} fuel cell diffusion media. *Electrochimica Acta*, 55(5):1619 – 1625, 2010.

[40] Manish Khandelwal and M.M. Mench. Direct measurement of through-plane thermal conductivity and contact resistance in fuel cell materials. *Journal of Power Sources*, 161(2):1106 – 1115, 2006.

[41] J. Kleemann, F. Finsterwalder, and W. Tillmetz. Characterisation of mechanical behaviour and coupled electrical properties of polymer electrolyte membrane fuel cell gas diffusion layers. *Journal of Power Sources*, 190(1):92 – 102, 2009.

[42] Woo kum Lee, Chien-Hsien Ho, J.W. Van Zee, and Mahesh Murthy. The effects of compression and gas diffusion layers on the performance of a {PEM} fuel cell. *Journal of Power Sources*, 84(1):45 – 51, 1999.

[43] Xinmin Lai, Dongan Liu, Linfa Peng, and Jun Ni. A mechanicalelectrical finite element method model for predicting contact resistance between bipolar plate and gas diffusion layer in {PEM} fuel cells. *Journal of Power Sources*, 182(1):153 – 159, 2008.

[44] Yeh-Hung Lai, Yongqiang Li, and Jeffrey A. Rock. A novel full-field experimental method to measure the local compressibility of gas diffusion media. *Journal of Power Sources*, 195(10):3215 – 3223, 2010.

[45] Robert F Landel and Lawrence E Nielsen. *Mechanical properties of polymers and composites*. CRC Press, 1993.

[46] {ASTM} International. Test method for thermal transmission properties of thermally conductive electrical insulation materials, 2011.

[47] X. Li. *Principles Of Fuel Cells*. Taylor & Francis Group, 2006.

[48] Jui-Hsiang Lin, Wei-Hung Chen, Yen-Ju Su, and Tse-Hao Ko. Effect of gas diffusion layer compression on the performance in a proton exchange membrane fuel cell. *Fuel*, 87(12):2420 – 2424, 2008.

[49] S. Litster, D. Sinton, and N. Djilali. Ex situ visualization of liquid water transport in {PEM} fuel cell gas diffusion layers. *Journal of Power Sources*, 154(1):95 – 105, 2006.

[50] Engineered Fibers Technology LLC. Spectracarb 2050a porous carbon-paper product information, 2013.

[51] Engineered Fibers Technology LLC. Toray carbon fiber paper {TGP-H}, 2013.

[52] J. Lobato, P. Caizares, M.A. Rodrigo, C. Ruiz-Lpez, and J.J. Linares. Influence of the teflon loading in the gas diffusion layer of pbi-based {PEM} fuel cells. *Journal of Applied Electrochemistry*, 38(6):793–802, 2008.

[53] Thomas J. Mason, Jason Millichamp, Tobias P. Neville, Ahmad El-kharouf, Bruno G. Pollet, and Daniel J.L. Brett. Effect of clamping pressure on ohmic resistance and compression of gas diffusion layers for polymer electrolyte fuel cells. *Journal of Power Sources*, 219(0):52 – 59, 2012.

[54] M Mathias, J Roth, J Fleming, and W Lehnert. *Handbook of Fuel Cells-Fundamentals, Technology and Applications, Vol. 3: Fuel Cell Technology and Application*. Wiley, New York, 2003.

[55] Virendra K. Mathur and Jim Crawford. Fundamentals of gas diffusion layers in {PEM} fuel cells. In Suddhasatwa Basu, editor, *Recent Trends in Fuel Cell Science and Technology*, pages 116–128. Springer New York, 2007.

[56] Toyoaki Matsuura, Megumi Kato, and Michio Hori. Study on metallic bipolar plate for proton exchange membrane fuel cell. *Journal of Power Sources*, 161(1):74 – 78, 2006.

[57] Viral Mehta and Joyce Smith Cooper. Review and analysis of {PEM} fuel cell design and manufacturing. *Journal of Power Sources*, 114(1):32 – 53, 2003.

[58] V. Mishra, F. Yang, and R. Pitchumani. Measurement and prediction of electrical contact resistance between gas diffusion layers and bipolar plate for applications to {PEM} fuel cells. *Journal of Fuel Cell Science and Technology*, 1(2):2–9, 2004.

[59] Hiroaki Narisawa, Masanobu Maeda, Minoru Hattori, and Masahiro Kaneko. Phenolic resin composition, December 16 2003. US Patent 6,664,343.

[60] I. Nitta, O. Himanen, and M. Mikkola. Thermal conductivity and contact resistance of compressed gas diffusion layer of {PEM} fuel cell. *Fuel Cells*, 8(2):111–119, 2008.

[61] Iwao Nitta, Olli Himanen, and Mikko Mikkola. Contact resistance between gas diffusion layer and catalyst layer of {PEM} fuel cell. *Electrochemistry Communications*, 10(1):47 – 51, 2008.

[62] Department of Energy Hydrogen and Fuel Cells Program Plan. An integrated strategic plan for the research, development, and demonstration of hydrogen and fuel cell technologies. Technical report, U.S. Department of Energy, September 2011.

[63] Anthony C. Okafor and Hector-Martins C. Magbo. Investigation of the effects of catalyst loading and gas flow rate on polymer electrolyte membrane {PEM} fuel cell performance and degradation. *Journal of Fuel Cell Science and Technology*, 9(011006), 2011.

[64] Andrews J. P Rama P., Chen R. A review of performance degradation and failure modes for hydrogen-fuelled polymer electrolyte fuel cells. *Journal of Power and Energy*, 222(5):421–441, 2008.

[65] N. Parikh, J. S. Allen, and R. S. Yassar. Microstructure of gas diffusion layers for {PEM} fuel cells. *Fuel Cells*, 12(3):382–390, 2012.

[66] Joel J. Pawlak and D. Steven Keller. The compressive response of a stratified fibrous structure. *Mechanics of Materials*, 37(11):1132 – 1142, 2005.

[67] Joshua Pelleg. *Mechanical properties of materials*, volume 190. Springer, 2012.

[68] Jichao Qiao, Zhengping Xi, Huiping Tang, Jianyong Wang, and Jilei Zhu. Influence of porosity on quasi-static compressive properties of porous metal media fabricated by stainless steel fibers. *Materials and Design*, 30(7):2737 – 2740, 2009.

[69] Vijay Radhakrishnan and Prathap Haridoss. Effect of cyclic compression on structure and properties of a gas diffusion layer used in {PEM} fuel cells. *International Journal of Hydrogen Energy*, 35(20):11107 – 11118, 2010.

[70] Vijay Radhakrishnan and Prathap Haridoss. Differences in structure and property of carbon paper and carbon cloth diffusion media and their impact on proton exchange membrane fuel cell flow field design. *Materials and Design*, 32(2):861 – 868, 2011.

[71] Julien Ramousse, Sophie Didierjean, Olivier Lottin, and Denis Maillet. Estimation of the effective thermal conductivity of carbon felts used as {PEMFC} gas diffusion layers. *International Journal of Thermal Sciences*, 47(1):1 – 6, 2008.

[72] E. Sadeghi, N. Djilali, and M. Bahrami. Effective thermal conductivity and thermal contact resistance of gas diffusion layers in proton exchange membrane fuel cells. part 2: Hysteresis effect under cyclic compressive load. *Journal of Power Sources*, 195(24):8104 – 8109, 2010.

[73] E. Sadeghi, N. Djilali, and M. Bahrami. Effective thermal conductivity and thermal contact resistance of gas diffusion layers in proton exchange membrane fuel cells. part 1: Effect of compressive load. *Journal of Power Sources*, 196(1):246 – 254, 2011.

[74] Hamidreza Sadeghifar, Ned Djilali, and Majid Bahrami. Effect of polytetrafluoroethylene (ptfe) and micro porous layer (mpl) on thermal conductivity of fuel cell gas diffusion layers: Modeling and experiments. *Journal of Power Sources*, 248(0):632 – 641, 2014.

[75] G Sala. Composite degradation due to fluid absorption. *Composites Part B: Engineering*, 31(5):357 – 373, 2000.

[76] R. Selzer and K. Friedrich. Mechanical properties and failure behaviour of carbon fibre-reinforced polymer composites under the influence of moisture. *Composites Part A: Applied Science and Manufacturing*, 28(6):595 – 604, 1997.

[77] Chi-Hung Shen and George S Springer. Effects of moisture and temperature on the tensile strength of composite materials. *Journal of Composite Materials*, 11(1):2–16, 1977.

[78] Z. Shi and X. Wang. Pore structure modeling of flow in gas diffusion layers of proton exchange membrane fuel cells. *ASME Conference Proceedings*, 9:525–531, 2010.

[79] Dusan Spernjak, Ajay K. Prasad, and Suresh G. Advani. Experimental investigation of liquid water formation and transport in a transparent single-serpentine {PEM} fuel cell. *Journal of Power Sources*, 170(2):334 – 344, 2007.

[80] Snezana B. Stankovic. Compression hysteresis of fibrous systems. *Polymer Engineering & Science*, 48(4):676–682, 2008.

[81] Z.Y. Su, C.T. Liu, H.P. Chang, C.H. Li, K.J. Huang, and P.C. Sui. A numerical investigation of the effects of compression force on {PEM} fuel cell performance. *Journal of Power Sources*, 183(1):182 – 192, 2008.

[82] John Summerscales. Composites design and manufacture (beng) - strength. failure mechanisms. fractography. failure criteria. fracture mechanics., 2014.

[83] A. Tamayol, F. McGregor, and M. Bahrami. Single phase through-plane permeability of carbon paper gas diffusion layers. *Journal of Power Sources*, 204(0):94 – 99, 2012.

[84] Starvos Tavoularis. 574:506, march 2007.

[85] John R. Taylor. *An Introduction to Error Analysis: The Study of Uncertainties in Physical Measurements*. University Science Books, 2 edition, 1997.

[86] Bourbie Thierry, Coussy Olivier, and Zinster Bernard. *Acoustics of Porous Media*. 1987.

[87] Grant Unsworth. Measurement and characterization of heat and mass diffusion in pemfc porous media. Master's thesis, University of Waterloo, Waterloo, Ontario, Canada.

[88] Grant Unsworth, Nada Zamel, and Xianguo Li. Through-plane thermal conductivity of the microporous layer in a polymer electrolyte membrane fuel cell. *International Journal of Hydrogen Energy*, 37(6):5161 – 5169, 2012.

[89] Valery V Vasiliev and Evgeny Morozov. *Mechanics and analysis of composite materials*. Elsevier, 2001.

[90] Y.M. Volfkovich, A.V. Sakars, and A.A. Volinsky. Application of the standard porosimetry method for nanomaterials. {*IJNT*}, 2(3):292, 2005.

[91] Yun Wang, Chao-Yang Wang, and K.S. Chen. Elucidating differences between carbon paper and carbon cloth in polymer electrolyte fuel cells. *Electrochimica Acta*, 52(12):3965 – 3975, 2007.

[92] Silvia [Ballard Materials Products] [Ballard Materials Products] Wessel and David [Ballard Materials Products] [Ballard Materials Products] Harvey. *Final Project Report: Development of Micro-Structural Mitigation Strategies for PEM Fuel Cells: Morphological Simulations and Experimental Approaches*. Jun 2013.

[93] Zhiliang Wu, Shuxin Wang, Lianhong Zhang, and S. Jack Hu. An analytical model and parametric study of electrical contact resistance in proton exchange membrane fuel cells. *Journal of Power Sources*, 189(2):1066 – 1073, 2009.

[94] Zhiliang Wu, Yuanyuan Zhou, Guosong Lin, Shuxin Wang, and S. Jack Hu. An improved model for predicting electrical contact resistance between bipolar plate and gas diffusion layer in proton exchange membrane fuel cells. *Journal of Power Sources*, 182(1):265 – 269, 2008.

[95] J. Yablecki and A. Bazylak. Modeling the effective thermal conductivity of an anisotropic gas diffusion layer in a polymer electrolyte membrane fuel cell. In {*ASME*} *2011 9th International Conference on Fuel Cell Science, Engineering and Technology*. {ASME}, 2011.

[96] Peiyun Yi, Linfa Peng, Xinmin Lai, and Jun Ni. A numerical model for predicting gas diffusion layer failure in proton exchange membrane fuel cells. *Journal of Fuel Cell Science and Technology*, 8:011011, 2011.

[97] Sung-Dae Yim, Byung-Ju Kim, Young-Jun Sohn, Young-Gi Yoon, Gu-Gon Park, Won-Yong Lee, Chang-Soo Kim, and Yong Chai Kim. The influence of stack clamping pressure on the performance of {PEM} fuel cell stack. *Current Applied Physics*, 10(2, Supplement):S59 – S61, 2010.

[98] Wonseok Yoon, Xinyu Huang, Paul Fazzino, Kenneth L. Reifsnider, and Michael A. Akkaoui. Evaluation of coated metallic bipolar plates for polymer electrolyte membrane fuel cells. *Journal of Power Sources*, 179(1):265 – 273, 2008.

[99] Y.H. Zhao, G.P. Tandon, and G.J. Weng. Elastic moduli for a class of porous materials. *Acta Mechanica*, 76(1-2):105–131, 1989.

[100] P. Zhou and C.W. Wu. Numerical study on the compression effect of gas diffusion layer on {PEMFC} performance. *Journal of Power Sources*, 170(1):93 – 100, 2007.

[101] P. Zhou, C.W. Wu, and G.J. Ma. Influence of clamping force on the performance of {PEMFCs}. *Journal of Power Sources*, 163(2):874 – 881, 2007.

[102] Y. Zhou, G. Lin, A.J. Shih, and S.J. Hu. A micro-scale model for predicting contact resistance between bipolar plate and gas diffusion layer in {PEM} fuel cells. *Journal of Power Sources*, 163(2):777 – 783, 2007.